# EFFECTS OF AGING AND REMODELING ON BONE MICRODAMAGE FORMATION

A Thesis
Presented to
The Academic Faculty

by

Jason Lee Wang

In Partial Fulfillment
of the Requirements for the Degree
Master of Science in the
School of Mechanical Engineering

Georgia Institute of Technology
December 2010

# EFFECTS OF AGING AND REMODELING ON BONE MICRODAMAGE FORMATION

Approved by:

Dr. Robert E. Guldberg, Advisor
School of Mechanical Engineering
*Georgia Institute of Technology*

Dr. Ken Gall
School of Mechanical Engineering
*Georgia Institute of Technology*

Dr. Rudolph L. Gleason
School of Mechanical Engineering
*Georgia Institute of Technology*

Date Approved: November 1, 2010

To my mom, dad, and sister for always supporting me

# ACKNOWLEDGEMENTS

First, I would like to thank my advisor Dr. Robert Guldberg. He took me on as an undergraduate in the fall of 2008 and gave me the opportunity to experience what conducting research is like. Over the past 3 years he has helped me to grow as a student and as a researcher, always guiding me in the right direction but allowing me to come to my own conclusions. He has also shown incredible faith in my ability to follow through with my work and has trusted in my potential to become a successful graduate student. I have learned so much about academic research from Dr. Guldberg, ranging from designing experiments to thinking outside of the box to technical writing. Through his summer and winter lab parties, he has also shown me that there is more to research than just the work. It is with the utmost gratitude that I thank him for all his past, present, and future support.

Next I would like to thank my other committee members, Dr. Ken Gall and Dr. Rudy Gleason. They provided invaluable insight as well as advice for further investigations. With their help I have realized how important it is to consider minute and seemingly inconsequential details.

I also must thank my fellow lab members as they have helped me tremendously with research, school, and life. The first person I met in the Guldberg lab was Angela Lin. As the unofficial guru of micro-CT and mechanical testing, she has helped me all throughout my graduate career with nearly every aspect of my experiments. Angela has always been there to provide her expert opinions and has never said no to helping me – or anyone, for that matter – out with anything. Jessica O'Neal has been my closest mentor

and friend as we both worked through the microdamage project. She taught me the methods and techniques that I needed and always pointed me in the right direction for extra assistance. Whether it was bonding over experimental mishaps or the hours spent in the dark microscope room searching for microdamage, Jessica has been someone to turn to for advice, ideas, and laughs. Without her help, I would not be where I am now, and for that, I owe her big time. Dr. Tamim Diab was also instrumental in my MS work. He provided his knowledge and research experience to make my work more polished as well as his personal experiences in academia to help me grow and find my own path. I am thankful for his constant willingness to provide me with his time and assistance. I would also like to thank Joel Boerckel and Nick Willett for their help with my statistics dilemma. Although we did not come up with a better solution, it helped me a great deal to go through the brainstorming session, and I appreciate their help. My gratitude goes to Hazel Stevens and Vivian Johnson for getting my orders out and for helping with miscellaneous lab issues.

I would like to thank the rest of the current Guldberg lab members. Chris Dosier I have to thank especially for our bonding time on the car ride to New Orleans. Ashley Allen has been a great row member in the lair and special thanks goes to her for our many attempts to go to Moe's. I also thank Brent Uhrig, Tanu Thote, and Alice Li for their assistance and company in the lab. I would also like to thank the previous Guldberg lab members who have helped me. Dr. Liqin Xie helped me run my first experiments and also helped me write my first abstract that allowed me to go to my first ORS conference. Dr. Ken Dupont shared with me his perspectives on school and research and has always been willing to give me his help. Dr. Yash Kolambkar shared with me his insights on life

after graduate school, and I always appreciate the conversations we have. Dr. Mela Johnson could always be heard laughing about something in the lair and brought a great positive energy to the lab. Thanks to Eric Deutsch for introducing me to cell culture (although I did not pursue it further) and for his perspectives on graduate school. Finally, thanks to Dr. Srin Nagaraja who paved the way for the microdamage research to be done in the lab.

I would like to thank Dr. Brani Vidakovic for his assistance with my statistics. He helped me understand the importance of conducting the right analysis. I must thank Aqua Asberry for her never ending assistance and company as I worked endless hours in the histology lab.

Finally, I want to thank my family and friends. My mom, dad, and sister have always been there for me and have always supported me, especially through my undergraduate and graduate career. I am forever indebted and grateful to them for their love and care. Thanks to all my friends who have been patient and understanding as I worked tirelessly in the lab and on my thesis. They have put up with my frustrations and venting, and I could not ask for better friends.

Thank you all for your support!

# TABLE OF CONTENTS

# LIST OF TABLES

Page

# LIST OF FIGURES

Page

# LIST OF ABBREVIATIONS

| | |
|---|---|
| ALN | Alendronate |
| ANOVA | Analysis of variance |
| BMD | Bone mineral density |
| BV/TV | Bone volume fraction |
| $BV/TV_{trab}$ | Trabecular bone volume fraction |
| $BV/TV_{whole}$ | Whole vertebra bone volume fraction |
| Conn.D | Connectivity Density |
| CSA | Cross sectional area |
| DA | Degree of anisotropy |
| FE | Finite element |
| HA | Hydroxyapatite |
| Micro-CT | Microcomputed tomography |
| MMA | Methyl methacrylate |
| MOI | Moment of inertia |
| OVX | Ovariectomy |
| PI | Protease inhibitor |
| RAL | Raloxifene |
| ROI | Region of interest |
| SERM | Selective estrogen receptor modulator |
| SMI | Structure model index |
| Tb.N | Trabecular number |
| Tb.Sp | Trabecular separation |
| Tb.Th | Trabecular thickness |

# SUMMARY

Skeletal fragility is characterized by low bone mass, negative changes in bone microarchitecture, and compromised tissue matrix properties, including accumulation of microdamage. Microdamage accumulates *in vivo* from daily physiological loading and is targeted for repair through a normal remodeling process, thus preventing microcrack growth and potential fracture. However, impaired remodeling is associated with aging and osteoporosis, resulting in an increased accumulation of microdamage which contributes to reduced bone mechanical properties. The current clinical method for assessing increased risk of fracture involves measuring bone mineral density (BMD) of the hip and spine, locations of trabecular bone where high rates of remodeling occur. The bisphosphonate alendronate (ALN) reduces clinical risk for fracture by significantly increasing BMD, but studies have shown a concomitant reduction in intrinsic properties that may be the underlying cause for recent reports of spontaneous fractures with long-term alendronate use. Another anti-resorptive agent called raloxifene (RAL) is a selective estrogen receptor modulator (SERM) and has been shown to modestly improve BMD while decreasing fracture risk to a similar degree as alendronate. The combination of RAL and ALN as a treatment for osteoporosis may provide the benefits of each drug without the negative effects of ALN.

Therefore, the overall goal of this thesis was to address the effects of aging and anti-resorptive agents on the properties of bone through the formation of microdamage. Assessment of age-related effects on bone was conducted through quantification of microdamage progression. It was found that old bone results in greater incidences of microdamage progression, reflecting a compromised tissue matrix with reduced

resistance to crack growth. Effects of combination treatment with RAL and ALN were evaluated through biomechanical testing, micro-CT imaging, and microdamage quantification. Results showed improved trabecular bone volume and ultimate load with positive effects on trabecular architecture. Combination treatment reduced the proportion of microdamage that may lead to catastrophic fracture, indicating an improvement in the local tissue matrix properties.

# CHAPTER 1

# INTRODUCTION

## Overview

Bone quality is dependent on many factors such as microarchitectural organization and the condition of the tissue matrix, including the accumulation of microdamage [1-2]. Compromised bone quality combined with decreases in bone mass contributes to increased skeletal fragility in humans. These changes in bone can lead to compromised function and potentially traumatic fractures – often in the hip, spine, and wrist where cancellous bone is most prevalent – as is seen with osteoporosis and the elderly population. In the United States alone, osteoporotic fractures were estimated to be greater than 2 million and cost nearly $17 billion in 2005 with a predicted rise in incidence and cost of nearly 50% by 2025 [3]. It is believed that the changes in bone quality associated with aging and osteoporosis are the cause for the resultant decreases in material properties that increase fracture risk [1, 4]. Current clinical methods measure bone mineral density (BMD) to predict fracture risk, but a study by Hui et al showed that at a given bone mass, fracture risk increases with age [5]. This reflects the lack of sensitivity this diagnostic measurement has to changes in bone quality such as increased microdamage accumulation [6]. Concomitantly, current therapies aim to increase bone mass through pharmacological means such as the anti-resorptive agents bisphosphonates and selective estrogen receptors (SERMs). Since no clinical methods have been established for measuring bone strength and bone quality to assess fracture risk to date, understanding the underlying changes leading to increased skeletal fragility may provide

the basis for new diagnostics and treatments. Therefore, the overall goal of this thesis was to provide insight into the properties of bone through the formation of microdamage and biomechanical testing as it pertains to aging and the use of anti-resorptive agents for treatment of osteoporosis in trabecular bone.

## Background

Bone is an integral component of our bodies, providing structural support and facilitating movement. Each bone sees a different mechanical environment depending on where it is located in the skeleton giving rise to the different shapes and sizes [7]. To adequately sustain the physiological forces subsequently imparted, two types of bone are present in varying ratios: cortical (compact) and trabecular (cancellous) bone. Cortical bone is dense bone with very low porosity that makes up about 80% of the adult human skeleton [8]. While primarily found in the diaphysis of long bones, cortical bone makes up the outer wall of all bones, thereby providing support and protection. The remaining 20% of the human skeleton consists of trabecular bone. Found in the metaphysis and epiphysis of long bones and in vertebrae, trabecular bone has a highly porous structure consisting of a network of trabecular plates and rods. Both cortical and trabecular bone consist of mineralized collagen fibrils laid down in a lamellar pattern [8-9]. This combination of organic and inorganic components arranged in a complex ordered fashion provides bone with the necessary stiffness and ductility to withstand variable modes of loading.

Unlike typical engineering materials, bone is a dynamic organ capable of restructuring itself in order to compensate for changes in local stresses and strains. This process is known as bone remodeling and involves three main cells: osteoclasts,

osteoblasts, and osteocytes [10]. The remodeling cycle begins with activation of osteoclasts and osteoblasts. Mature osteoclasts then resorb bone followed by osteoblasts which deposit unmineralized bone matrix (osteoid) to be slowly mineralized over time. Osteoblasts incorporated into the bone matrix are called osteocytes and are believed to be integral to the activation of the remodeling process [11]. Bone remodeling can also be initiated by osteocytes as a result of microcrack formation [12-13]. These cracks, if left unrepaired, accumulate and could lead to fractures and thus compromise the integrity of the bone [14].

However, the presence of microdamage is not an indication of imminent failure of bone. In 1960, Harold Frost was the first to demonstrate that microcracks developed *in vivo* due to fatigue in his study looking at human ribs [15]. Since then, many researchers have shown that microcracks form *in vivo* in cortical [16-18] and trabecular bone [19-22]. This microdamage forms as a consequence of daily physiological loading in the form of fatigue. Bone remodeling then occurs as a response to this fatigue damage in an effort to repair the bone [23]. Burr and associates showed in dogs that microdamage formed as a consequence of *in vivo* loading and remodeling occurred as a response to it [24-25]. A study in rat ulna showed that intracortical remodeling activated as a result of fatigue microdamage even though laboratory rats are understood to lack haversian remodeling activity [26]. The balance between microdamage formation and repair is what allows bone to maintain its mechanical integrity [27].

While microdamage accumulation is considered to contribute to skeletal fragility, its exact role in increasing fracture risk is not entirely understood [28-29]. Many studies have been conducted to investigate microdamage accumulation with age [17, 19, 22, 30]

and its role in bone mechanical properties. Mori et al found that microcrack density increased significantly with age but that women with fractures did not have more microdamage than women without fractures [19]. While this indicates no direct relationship between microdamage accumulation and fractures, there is no data regarding tissue matrix properties or trabecular architecture accompanying this study. Damage in trabecular bone was found to form at strains below apparent yield strain as determined from reductions in modulus [31]. Others have found that significant levels of microdamage do not form until apparent yield strains are reached or exceeded [32-34]. Interestingly, the presence of microdamage in trabecular bone seems to play a greater role in decreases in apparent mechanical properties than do trabecular fractures [35]. In any case, strain induced microdamage formation is strongly correlated with strain induced reductions in modulus and strength [32, 36]. Results from Burr et al also showed this relationship with the presence of microcrack accumulation in cortical bone after a stiffness loss of 15% [37]. In fact, differences in modulus loss with aging have been shown to reflect a longer fatigue life for younger bone [38]. A study in young human vertebrae showed a decrease in energy absorption associated with increasing density of microcracks [39]. With increasing age, accumulation of microdamage was found to be associated more with changes in toughness properties than with stiffness or strength [18]. This data suggests a strong relationship between microdamage and bone mechanical properties. However other factors should not be ignored when considering microdamage and the mechanical properties of bone. For instance, Bevill et al showed variability in yield strains with respect to loading-axis between human trabecular bone in vertebral bodies and femoral necks [40]. Arlot et al showed that in human vertebrae, microdamage

increases with age exponentially and is associated with a more rod-like trabecular architecture [41]. These studies necessitate understanding of bone location and architecture in addition to microdamage and bone mass in order to adequately characterize bone material properties. Similarly, the hierarchical nature of bone and the role of the tissue matrix should not be ignored when studying microdamage [42].

The behavior of microdamage in bone also provides insight into the role of microcracks in skeletal fragility. Biomechanical testing of bone has shown that two types of microdamage form: linear and diffuse [43-45]. Linear type damage is associated more with bone in tension while diffuse damage is typically found in compressive regions. Burr et al found that cracks tended to be fewer and longer in compressive than tensile cortices [37]. Reilly and Currey found this same result and also noted that areas in tension formed cracks at lower strains than areas in compression, but once formed, compressive microcracks tended to grow into long cracks [43]. This behavior suggests that diffuse damage is self limiting and thus is less deleterious to the mechanical integrity of bone [46]. In fact, linear damage is associated more with older bone and a lower fatigue life [46] and exhibits more targeted remodeling than diffuse damage [45]. Compressive damage was also shown to drastically reduce the energy absorption capacity of bone [47]. The nature of crack formation in bone would indicate that bone is formed specifically to withstand a single mode of loading [43, 47].

The danger of linear damage is in its propensity to rapidly propagate and cause catastrophic fracture [37], especially in the absence of microstructural barriers [48]. Thus in order to elucidate the contribution of microdamage to fracture risk, it is important to determine how and why cracks propagate and are arrested in bone. It is understood that

cracks initiate at areas of stress concentration (e.g. bone surfaces, cement lines, canal networks) and will subsequently grow according to the path of least resistance [48-50]. Vashishth et al suggested a pattern for crack growth involving the formation of a small zone of cracks due to applied loads followed by a main crack that accelerates through this zone and slows at areas of undamaged matrix [51]. Further loading causes this main crack to slowly propagate as smaller microcracks form behind and in front it at which point the pattern repeats again. Given that loads are continuously applied, this crack growth may or may not accelerate through bone to fracture with a dependence on crack size when obstacles are encountered [48]. However, bone is naturally a fatigue resistant composite material predisposed to resisting crack propagation [37, 52] through various mechanisms including crack bridging, crack deflection, and the creation of more cracks [53]. These findings apply to cortical bone which is much more dense and structured than the highly porous trabecular bone. Thus, while in principle these ideas apply to trabecular bone, the exact behavior of microcracks in trabecular bone has not been well studied. Wang et al utilized shear and compressive loading to test young bovine tibial cancellous bone for microdamage propagation [54]. They found that mixed mode loading resulted in microcrack propagation, implying a propensity for trabecular bone to allow crack propagation. In a finite element study, trabecular bone was found to fail (defined as 30% modulus reduction) as a result of an accumulation of microcracks and not trabecular fractures [55]. This indicates preference towards creation of more microdamage versus propagation of existing cracks. However this model only included compressive loads and assumed homogeneous tissue properties. Regardless of the type of bone, microdamage behavior changes as a result of changes in tissue matrix properties as seen with aging and

osteoporosis. As bone ages, the tissue becomes more mineralized and homogeneous. This reduces the ability of bone to resist both crack initiation and crack growth [56-57]. Thus a more mineralized tissue matrix combined with imbalanced remodeling due to aging results in microdamage accumulation and increased risk for crack propagation to catastrophic failure [29, 38].

Many methods have been developed in order to detect microdamage in bone both *in vivo* and *in vitro* including chelating fluorochromes [58]. Unlike the basic fuchsin label used by Frost [15] and later validated by Burr and Stafford [59], fluorochromes such as alizarin and calcein are site-specific and have a range of emission wavelengths ideal for detecting a series of microcrack events [58]. Lee et al was the first to report the technique of sequentially labeling microcracks *in vitro* with chelating fluorochromes [60]. However the stains used were not easily separable visually and also raised concerns of dye substitution. Later O'Brien et al improved upon this technique by analyzing the affinity of several chelating agents for calcium ions effectively reducing the possibility of dye substitution by defining an optimal sequence of staining [61]. Since then, many studies have utilized this technique for varying purposes including to correlate microdamage to microstructural stresses in bovine trabecular bone [62], to look at microdamage propagation in bovine trabecular bone [54], to examine age related responses of rat trabecular bone to microdamage [63], to measure microdamage accumulation in human vertebral trabecular bone [41], and to relate microdamage initiation with microstructural stresses in alendronate treated dogs [64].

Clinically, investigating the role of microdamage accumulation in fracture risk may provide clinicians with improved diagnostic tools and alternative therapies to drugs

such as bisphosphonates and selective estrogen receptor modulators (SERMs). Bisphosphonates are pharmacological compounds that bind strongly to the mineral in bone, hydroxyapatite [65]. During resorption of bone, bisphosphonates are internalized by osteoclasts and subsequently induce apoptosis of the osteoclasts. The result is an inhibition of bone resorption and an increase in bone mineral density. Alendronate (ALN), a bisphosphonate used clinically, has been shown to increase BMD from base-line values in postmenopausal women with osteoporosis in the lumbar spine (13.7%), trochanter (10.3%), femoral neck (5.4%), and at the total proximal femur (6.7%) [66]. It has also been shown to reduce the risk of clinical fractures in women without vertebral fractures with osteoporosis by 36% [67]. Another study reported increases in the mean degree of mineralization of bone with alendronate treatment for 2 and 3 years and a subsequent increase in BMD and reduction in fracture rate [68]. SERMs are partial agonists that bind to estrogen receptors and like bisphosphonates, inhibit resorption of bone resulting in an increase in bone mass but to a lesser degree than bisphosphonates [69]. Raloxifene (RAL) is a clinically available SERM that has been shown in a four year study of women with postmenopausal osteoporosis to decrease the vertebral fracture risk by 39% and modestly improve BMD in both the lumbar spine and femoral neck (<3%) compared to placebo [70]. Other studies have shown the ALN increases BMD by a significantly greater amount than RAL in postmenopausal women with low BMD, but no analysis of fracture risk was conducted [71-72]. Thus presents a paradox in which RAL increases BMD to a lesser degree than ALN but reduces fracture risk by a comparable amount [73]. Clearly BMD is not the only factor involved in determining fracture risk as

evidenced by the 17% and 4% contributions BMD provides to reductions in vertebral fracture risk with ALN and RAL therapy, respectively [6, 73].

Animal studies have utilized clinically relevant doses of both RAL and ALN to investigate effects on both bone mechanical properties and on microdamage accumulation. In a study in beagles, ALN doses equivalent to 6 times the recommended clinical dosage were administered to investigate the effects of suppressed bone turnover [74]. The group's previous study indicated microdamage accumulation in the rib cortex accompanied by a reduction in bone toughness. This subsequent study found significant increases in microdamage accumulation in the vertebrae as well as increased trabecular bone volume and vertebral strength. They also found a 21% reduction in vertebral toughness, indicating a relationship with microdamage. However, later studies by Allen et al with clinically relevant doses of ALN administered to beagles found no changes in vertebral mechanical properties except an increase in stiffness despite an increase in microdamage accumulation from control [75]. The lack of reduction in mechanical properties was attributed to the significant increases in bone volume and mineralization. A follow up study carried the treatment through to 3 years and found no differences in microdamage accumulation in vertebrae or decreased vertebral toughness when compared with beagles treated for one year [76]. A similar study found no differences in any mechanical properties in canine femoral cortical bone as a result of ALN treatment between 1 and 3 years of treatment [77]. It seems that treatment with ALN may reduce fracture risk primarily through drastically reduced remodeling related increases in bone mass and mineralization. In contrast, treatment with clinically relevant doses of RAL for one year in beagles resulted in no increase in microdamage accumulation and a

significant increase in vertebral strength when compared to vehicle treated beagles [78]. A continuation of this study found that RAL treatment increased ultimate stress, modulus, and toughness values in trabecular bone and toughness values in cortical bone over vehicle treated dogs [79]. Treatment with ALN or RAL each has its pros and cons, thus leading to a reasonable avenue for investigation regarding the combination of the two as a treatment modality. Johnell et al conducted a study to determine the additive effects of ALN and RAL and found that the combination of the two anti-resorptive drugs resulted in a greater reduction in bone turnover and greater BMD in the femoral neck [80]. However no biomechanical tests were conducted and thus no effects on mechanical properties are known. If the effects of RAL and ALN are additive in BMD, then it would be safe to hypothesize a similar result when examining the effects of combination treatment on bone mechanical properties.

## Specific Aims

The overall goal of this thesis was to determine the integrity of bone tissue through biomechanical testing and microdamage quantification. Bone matrix properties are integral to understanding skeletal fragility. Mechanical testing data can be used to determine derived material properties which reflect the behavior of bone at the apparent level. Analyzing the amount of microdamage present in bone reflects tissue matrix properties and thus gives insight into the behavior of bone at the local level. This research is novel because it investigates the poorly understood nature of microdamage progression within trabecular bone as it relates to aging, and it evaluates the combination of raloxifene (RAL) and alendronate (ALN) on bone material properties as it may relate to

treatment for osteoporosis. It is significant because it seeks to utilize microdamage quantification as a means for assessing bone tissue matrix quality.

**Aim 1:**

*Quantify microdamage progression in human trabecular bone as a function of age*. Human trabecular bone from female donors was mechanically tested following a protocol developed by the researcher. Two separate loading conditions were applied to create microdamage and microdamage progression. An established fluorescent labeling technique was used to detect and differentiate initial microdamage from microdamage progression. Micro-CT imaging provided trabecular architecture and mineralization for analysis of age effects. It was hypothesized that bone from older donors would have increased incidence of microdamage and microdamage progression reflecting the propensity of older bone to form cracks *in vivo*.

**Aim 2:**

*Determine the effects of anti-resorptive agents on biomechanical properties in rat bone and microdamage formation in rat trabecular bone*. An established osteoporosis model in rats was used to determine effects of treatment with RAL, ALN, and the combination of the two. Rat femurs and vertebrae were mechanically tested to determine structural and derived material properties. A separate group of vertebrae were mechanically tested to induce microdamage formation. Fluorescent staining was applied as in Aim 1 to identify preexisting and test induced microdamage. Micro-CT imaging was used to determine morphological parameters of femurs and vertebrae. It was hypothesized that combination treatment with RAL and ALN would improve biomechanical properties in both the femurs and vertebrae more than each drug alone.

This would be a result of the additive effects of the increase in bone volume by ALN and the improvement of material properties by RAL. It was further hypothesized that microdamage accumulation would be greatest with ALN treatment among the treatment groups followed by combination treatment and RAL.

## References


1. McDonnell, P., P.E. McHugh, and D. O'Mahoney, *Vertebral osteoporosis and trabecular bone quality.* Ann Biomed Eng, 2007. **35**(2): p. 170-89.

2. Hernandez, C.J. and T.M. Keaveny, *A biomechanical perspective on bone quality.* Bone, 2006. **39**(6): p. 1173-81.

3. Burge, R., et al., *Incidence and economic burden of osteoporosis-related fractures in the United States, 2005-2025.* J Bone Miner Res, 2007. **22**(3): p. 465-75.

4. Burr, D.B., *The contribution of the organic matrix to bone's material properties.* Bone, 2002. **31**(1): p. 8-11.

5. Hui, S.L., C.W. Slemenda, and C.C. Johnston, Jr., *Age and bone mass as predictors of fracture in a prospective study.* J Clin Invest, 1988. **81**(6): p. 1804-9.

6. Seeman, E., *Is a change in bone mineral density a sensitive and specific surrogate of anti-fracture efficacy?* Bone, 2007. **41**(3): p. 308-17.

7. Seeman, E., *Bone quality: the material and structural basis of bone strength.* J Bone Miner Metab, 2008. **26**(1): p. 1-8.

8. Clarke, B., *Normal bone anatomy and physiology.* Clin J Am Soc Nephrol, 2008. **3 Suppl 3**: p. S131-9.

9. Weiner, S., W. Traub, and H.D. Wagner, *Lamellar bone: structure-function relations.* J Struct Biol, 1999. **126**(3): p. 241-55.

10. Robling, A.G., A.B. Castillo, and C.H. Turner, *Biomechanical and molecular regulation of bone remodeling.* Annu Rev Biomed Eng, 2006. **8**: p. 455-98.

11. Bonewald, L.F., *Mechanosensation and Transduction in Osteocytes.* Bonekey Osteovision, 2006. **3**(10): p. 7-15.

12. Verborgt, O., G.J. Gibson, and M.B. Schaffler, *Loss of osteocyte integrity in association with microdamage and bone remodeling after fatigue in vivo.* J Bone Miner Res, 2000. **15**(1): p. 60-7.

13. Hazenberg, J.G., et al., *Microdamage detection and repair in bone: fracture mechanics, histology, cell biology.* Technol Health Care, 2009. **17**(1): p. 67-75.

14. Martin, B., *Mathematical model for repair of fatigue damage and stress fracture in osteonal bone.* J Orthop Res, 1995. **13**(3): p. 309-16.

15. Frost, H.M., *Presence of microscopic cracks in vivo in bone.* Henry Ford Hospital Medical Bulletin, 1960. **8**: p. 25-35.

16. Donahue, S.W., et al., *Bone strain and microcracks at stress fracture sites in human metatarsals.* Bone, 2000. **27**(6): p. 827-33.

17. Schaffler, M.B., K. Choi, and C. Milgrom, *Aging and matrix microdamage accumulation in human compact bone.* Bone, 1995. **17**(6): p. 521-25.

18. Zioupos, P., *Accumulation of in-vivo fatigue microdamage and its relation to biomechanical properties in ageing human cortical bone.* J Microsc, 2001. **201**(Pt 2): p. 270-8.

19. Mori, S., et al., *Trabecular bone volume and microdamage accumulation in the femoral heads of women with and without femoral neck fractures.* Bone, 1997. **21**(6): p. 521-6.

20. Wenzel, T.E., M.B. Schaffler, and D.P. Fyhrie, *In vivo trabecular microcracks in human vertebral bone.* Bone, 1996. **19**(2): p. 89-95.

21. Fazzalari, N.L., et al., *Three-dimensional confocal images of microdamage in cancellous bone.* Bone, 1998. **23**(4): p. 373-8.

22. Fazzalari, N.L., et al., *Assessment of cancellous bone quality in severe osteoarthrosis: bone mineral density, mechanics, and microdamage.* Bone, 1998. **22**(4): p. 381-8.

23. Burr, D.B., *Targeted and nontargeted remodeling.* Bone, 2002. **30**(1): p. 2-4.

24. Burr, D.B., et al., *Bone remodeling in response to in vivo fatigue microdamage.* J Biomech, 1985. **18**(3): p. 189-200.

25. Mori, S. and D.B. Burr, *Increased intracortical remodeling following fatigue damage.* Bone, 1993. **14**(2): p. 103-9.

26. Bentolila, V., et al., *Intracortical remodeling in adult rat long bones after fatigue loading.* Bone, 1998. **23**(3): p. 275-81.

27. Martin, R.B., *Fatigue microdamage as an essential element of bone mechanics and biology.* Calcif Tissue Int, 2003. **73**(2): p. 101-7.

28. Burr, D.B., et al., *Bone microdamage and skeletal fragility in osteoporotic and stress fractures.* J Bone Miner Res, 1997. **12**(1): p. 6-15.

29. Burr, D., *Microdamage and bone strength.* Osteoporos Int, 2003. **14 Suppl 5**: p. S67-72.

30. Fazzalari, N.L., J.S. Kuliwaba, and M.R. Forwood, *Cancellous bone microdamage in the proximal femur: influence of age and osteoarthritis on damage morphology and regional distribution.* Bone, 2002. **31**(6): p. 697-702.

31. Morgan, E.F., O.C. Yeh, and T.M. Keaveny, *Damage in trabecular bone at small strains.* Eur J Morphol, 2005. **42**(1-2): p. 13-21.

32. Wachtel, E.F. and T.M. Keaveny, *Dependence of trabecular damage on mechanical strain.* J Orthop Res, 1997. **15**(5): p. 781-7.

33. Arthur Moore, T.L. and L.J. Gibson, *Microdamage accumulation in bovine trabecular bone in uniaxial compression.* J Biomech Eng, 2002. **124**(1): p. 63-71.

34. Moore, T.L. and L.J. Gibson, *Fatigue microdamage in bovine trabecular bone.* J Biomech Eng, 2003. **125**(6): p. 769-76.

35. Yeh, O.C. and T.M. Keaveny, *Relative roles of microdamage and microfracture in the mechanical behavior of trabecular bone.* J Orthop Res, 2001. **19**(6): p. 1001-7.

36. Keaveny, T.M., et al., *Mechanical behavior of damaged trabecular bone.* J Biomech, 1994. **27**(11): p. 1309-18.

37. Burr, D.B., et al., *Does microdamage accumulation affect the mechanical properties of bone?* J Biomech, 1998. **31**(4): p. 337-45.

38. Diab, T., et al., *Age-dependent fatigue behaviour of human cortical bone.* Eur J Morphol, 2005. **42**(1-2): p. 53-9.

39. Lu, W.W., et al., *Microfracture and changes in energy absorption to fracture of young vertebral cancellous bone following physiological fatigue loading.* Spine (Phila Pa 1976), 2004. **29**(11): p. 1196-201; discussion 1202.

40. Bevill, G., F. Farhamand, and T.M. Keaveny, *Heterogeneity of yield strain in low-density versus high-density human trabecular bone.* J Biomech, 2009. **42**(13): p. 2165-70.

41. Arlot, M.E., et al., *Microarchitecture influences microdamage accumulation in human vertebral trabecular bone.* J Bone Miner Res, 2008. **23**(10): p. 1613-8.

42. Vashishth, D., *Hierarchy of Bone Microdamage at Multiple Length Scales.* Int J Fatigue, 2007. **29**(6): p. 1024-1033.

43. Reilly, G.C. and J.D. Currey, *The development of microcracking and failure in bone depends on the loading mode to which it is adapted.* J Exp Biol, 1999. **202**(Pt 5): p. 543-52.

44. Diab, T. and D. Vashishth, *Effects of damage morphology on cortical bone fragility.* Bone, 2005. **37**(1): p. 96-102.

45. Herman, B.C., et al., *Activation of bone remodeling after fatigue: differential response to linear microcracks and diffuse damage.* Bone, 2010. **47**(4): p. 766-72.

46. Diab, T., et al., *Age-related change in the damage morphology of human cortical bone and its role in bone fragility.* Bone, 2006. **38**(3): p. 427-31.

47. Reilly, G.C. and J.D. Currey, *The effects of damage and microcracking on the impact strength of bone.* J Biomech, 2000. **33**(3): p. 337-43.

48. O'Brien, F.J., D. Taylor, and T. Clive Lee, *The effect of bone microstructure on the initiation and growth of microcracks.* J Orthop Res, 2005. **23**(2): p. 475-80.

49. Zarrinkalam, K.H., et al., *New insights into the propagation of fatigue damage in cortical bone using confocal microscopy and chelating fluorochromes.* Eur J Morphol, 2005. **42**(1-2): p. 81-90.

50. Voide, R., et al., *Time-lapsed assessment of microcrack initiation and propagation in murine cortical bone at submicrometer resolution.* Bone, 2009. **45**(2): p. 164-73.

51. Vashishth, D., K.E. Tanner, and W. Bonfield, *Contribution, development and morphology of microcracking in cortical bone during crack propagation.* J Biomech, 2000. **33**(9): p. 1169-74.

52. Akkus, O. and C.M. Rimnac, *Cortical bone tissue resists fatigue fracture by deceleration and arrest of microcrack growth.* J Biomech, 2001. **34**(6): p. 757-64.

53. Nalla, R.K., et al., *Fracture in human cortical bone: local fracture criteria and toughening mechanisms.* J Biomech, 2005. **38**(7): p. 1517-25.

54. Wang, X. and G.L. Niebur, *Microdamage propagation in trabecular bone due to changes in loading mode.* J Biomech, 2006. **39**(5): p. 781-90.

55. Kosmopoulos, V., C. Schizas, and T.S. Keller, *Modeling the onset and propagation of trabecular bone microdamage during low-cycle fatigue.* J Biomech, 2008. **41**(3): p. 515-22.

56. Nalla, R.K., et al., *Effect of aging on the toughness of human cortical bone: evaluation by R-curves.* Bone, 2004. **35**(6): p. 1240-6.

57. Zioupos, P., *In vivo fatigue microcracks in human bone: material properties of the surrounding bone matrix.* Eur J Morphol, 2005. **42**(1-2): p. 31-41.

58. Lee, T.C., et al., *Detecting microdamage in bone.* J Anat, 2003. **203**(2): p. 161-72.

59. Burr, D.B. and T. Stafford, *Validity of the bulk-staining technique to separate artifactual from in vivo bone microdamage.* Clin Orthop Relat Res, 1990(260): p. 305-8.

60. Lee, T.C., et al., *Sequential labelling of microdamage in bone using chelating agents.* J Orthop Res, 2000. **18**(2): p. 322-5.

61. O'Brien, F.J., D. Taylor, and T.C. Lee, *An improved labelling technique for monitoring microcrack growth in compact bone.* J Biomech, 2002. **35**(4): p. 523-6.

62. Nagaraja, S., T.L. Couse, and R.E. Guldberg, *Trabecular bone microdamage and microstructural stresses under uniaxial compression.* J Biomech, 2005. **38**(4): p. 707-16.

63. Waldorff, E.I., S.A. Goldstein, and B.R. McCreadie, *Age-dependent microdamage removal following mechanically induced microdamage in trabecular bone in vivo.* Bone, 2007. **40**(2): p. 425-32.

64. O'Neal, J.M., et al., *One year of alendronate treatment lowers microstructural stresses associated with trabecular microdamage initiation.* Bone, 2010. **47**(2): p. 241-7.

65. Russell, R.G., et al., *Mechanisms of action of bisphosphonates: similarities and differences and their potential influence on clinical efficacy.* Osteoporos Int, 2008. **19**(6): p. 733-59.

66. Bone, H.G., et al., *Ten years' experience with alendronate for osteoporosis in postmenopausal women.* N Engl J Med, 2004. **350**(12): p. 1189-99.

67. Cummings, S.R., et al., *Effect of alendronate on risk of fracture in women with low bone density but without vertebral fractures: results from the Fracture Intervention Trial.* JAMA, 1998. **280**(24): p. 2077-82.

68. Boivin, G.Y., et al., *Alendronate increases bone strength by increasing the mean degree of mineralization of bone tissue in osteoporotic women.* Bone, 2000. **27**(5): p. 687-94.

69. Kloosterboer, H.J. and A.G. Ederveen, *Pros and cons of existing treatment modalities in osteoporosis: a comparison between tibolone, SERMs and estrogen (+/-progestogen) treatments.* J Steroid Biochem Mol Biol, 2002. **83**(1-5): p. 157-65.

70. Delmas, P.D., et al., *Efficacy of raloxifene on vertebral fracture risk reduction in postmenopausal women with osteoporosis: four-year results from a randomized clinical trial.* J Clin Endocrinol Metab, 2002. **87**(8): p. 3609-17.

71. Sambrook, P.N., et al., *Alendronate produces greater effects than raloxifene on bone density and bone turnover in postmenopausal women with low bone density: results of EFFECT (Efficacy of FOSAMAX versus EVISTA Comparison Trial) International.* J Intern Med, 2004. **255**(4): p. 503-11.

72. Recker, R.R., et al., *Comparative effects of raloxifene and alendronate on fracture outcomes in postmenopausal women with low bone mass.* Bone, 2007. **40**(4): p. 843-51.

73. Riggs, B.L. and L.J. Melton, 3rd, *Bone turnover matters: the raloxifene treatment paradox of dramatic decreases in vertebral fractures without commensurate increases in bone density.* J Bone Miner Res, 2002. **17**(1): p. 11-4.

74. Mashiba, T., et al., *Effects of suppressed bone turnover by bisphosphonates on microdamage accumulation and biomechanical properties in clinically relevant skeletal sites in beagles.* Bone, 2001. **28**(5): p. 524-31.

75. Allen, M.R., et al., *Alterations in canine vertebral bone turnover, microdamage accumulation, and biomechanical properties following 1-year treatment with clinical treatment doses of risedronate or alendronate.* Bone, 2006. **39**(4): p. 872-9.

76. Allen, M.R. and D.B. Burr, *Three years of alendronate treatment results in similar levels of vertebral microdamage as after one year of treatment.* J Bone Miner Res, 2007. **22**(11): p. 1759-65.

77. Burr, D.B., et al., *Effects of 1 to 3 years' treatment with alendronate on mechanical properties of the femoral shaft in a canine model: implications for subtrochanteric femoral fracture risk.* J Orthop Res, 2009. **27**(10): p. 1288-92.

78. Allen, M.R., et al., *Raloxifene enhances vertebral mechanical properties independent of bone density.* Bone, 2006. **39**(5): p. 1130-5.

79. Allen, M.R., et al., *Raloxifene enhances material-level mechanical properties of femoral cortical and trabecular bone.* Endocrinology, 2007. **148**(8): p. 3908-13.

80. Johnell, O., et al., *Additive effects of raloxifene and alendronate on bone density and biochemical markers of bone remodeling in postmenopausal women with osteoporosis.* J Clin Endocrinol Metab, 2002. **87**(3): p. 985-92.

# CHAPTER 2

# AGE-RELATED CHANGES IN MICRODAMAGE PROGRESSION IN HUMAN TRABECULAR BONE

## Introduction

Bone mass in humans naturally increases until it reaches its peak at approximately 30 years of age [1]. Bone mass is maintained until about 40 years when a slow decline occurs resulting in the onset of osteopenia and eventually for many, especially postmenopausal women, osteoporosis. However these are not the only changes in bone that occur with age. Trabecular bone quality (collagen, mineral, and microdamage) [2-4], quantity (bone volume fraction), and microarchitecture (trabecular number, thickness, structure model index, etc.) are altered as a result of age-related changes [5-8]. It has been well established that the mineral content of bone contributes to strength and stiffness while the nature of the organic matrix has been largely disregarded. Recent studies have shown that decreases in the mechanical integrity in the collagen network result in compromised matrix properties and thus contribute to skeletal fragility [2-4]. Age-related reductions in bone volume fraction manifest themselves in more rod-like trabeculae, decreased thickness, and increased anisotropy [7-9]. These changes lead to decreases in the mechanical properties of bone and contribute to increased fracture risk.

Microdamage also contributes to the integrity of the bone tissue matrix and is known to accumulate with increasing age [10-13]. Testing of bone samples has shown that this microdamage contributes to decreases in biomechanical properties including

strength, stiffness, and toughness [14-17]. However microdamage is a naturally occurring process that occurs *in vivo* [18] and is considered to activate a targeted remodeling process [19]. Therefore, the accumulation of microdamage is associated with slow or suppressed remodeling that concomitantly results in increased bone tissue age and increased mineralization [4, 20-21]. It is believed that the homogeneous nature of the mineralized matrix due to improper remodeling allows crack propagation to occur [22-23]. This is because bone is naturally a composite material that provides natural barriers to crack growth [24]. Microdamage progression could also occur as a result of the accumulation of microdamage. Since damage is not repaired as efficiently, there is an increased presence of microcracks susceptible to crack growth which may lead to complete fracture [25]. While the exact role of microdamage in determining fracture risk is unclear, it is understood that it contributes to the decreases in bone mechanical properties and the maintenance of proper bone function through repair and remodeling [21, 26].

The goal of this aim was to determine the changes in microdamage progression in old bone versus young bone. It was hypothesized that due to the increased propensity of older bone to form microdamage *in vivo*, there would be a greater incidence of microdamage progression in old females when compared to young females.

## Materials and Methods

### Specimen Preparation

Fresh frozen trabecular bone specimens were harvested from the distal femur of six human female cadavers and divided into two groups: young (ages 29, 32, and 42) and old (ages 71, 77, and 82) (n = 3 per group). The researcher was blinded to these groups

until post-hoc analysis. Donors did not have any known history of metabolic bone diseases, osteoporotic fractures, or metastatic cancers. Cylindrical cores 5 mm in diameter were extracted from each donor under constant irrigation such that the principal material direction was approximately aligned with the loading axis. Samples were wrapped in saline soaked Kimwipes and stored at -20°C until needed [27]. One core from each donor (n = 3 cores/group) was selected and allowed to thaw overnight at 4°C prior to preparation for testing. Using a diamond saw (Isomet 1000 Precision Saw, Buehler Ltd., USA), cores were sized to a final length of 18 mm. Trabecular specimens were cleaned of marrow using a water-pik (WP-72W, WaterPik, USA) to minimize artifacts in microcomputed tomography (micro-CT) scans and to improve fluorescent stain penetration. Samples were then glued into custom stainless steel endcaps to reduce end artifacts during mechanical testing [28], resulting in an effective gauge length of 13 mm [29].

**Micro-CT Imaging**

Using a micro-CT system (μCT 40, Scanco Medical, Bassersdorf, Switzerland), each sample was scanned in the region between the top and bottom endcaps at a voxel resolution of 16 μm. A threshold was chosen to isolate bone from the background and any remaining soft tissue. Using built-in scanner software, bone volume fraction (BV/TV), degree of anisotropy (DA), bone mineralization (measured in mg-HA/$cm^3$), and trabecular architecture parameters were determined. Microarchitecture parameters included trabecular number (Tb.N, $mm^{-1}$), trabecular thickness (Tb.Th, mm), trabecular spacing (Tb.Sp, mm), connectivity density (Conn.D, $mm^{-3}$) and structural model index

(SMI). All samples were scanned in a 0.9% physiological saline solution with 10 μmol/L protease inhibitor (PI, E-64, Sigma Chemical) to retard tissue degradation.

**Mechanical Testing**

After micro-CT imaging, all specimens were loaded following two different protocols using a servo-hydraulic mechanical testing system (Mini Bionix 858, MTS Corp.). To ensure the presence of microcracks within each sample, the first test used a modified stress relaxation test [30]. Following nondestructive preconditioning for 3 cycles to 0.1% strain, samples were loaded under uniaxial compression at a rate of 0.5% strain/s to 0.8% strain and held at constant strain for 3 hours. Young's modulus was measured as the best linear fit of the ramp-up to 0.8% strain. Apparent strains were calculated using the displacement output from the testing system and the effective gauge length of the specimen measured using digital calipers.

In the second test, samples were mechanically tested in cyclic compression under load control according to a protocol adapted and modified from literature [31-32]. Specimens were preconditioned by loading under displacement control using a sinusoidal waveform for 10 cycles between 0.0% strain to 0.5% strain at a frequency of 2 Hz. This strain value falls below the yield strain determined during preliminary tests (1.1% strain) and was not expected to produce any microdamage [33]. The initial modulus, $E_0$, was defined as the slope of the best linear fit of the tenth loading cycle. This value was then used with the preload value (10 N) to define the maximum load corresponding to the normalized stress level, $\Delta\sigma/E_0 = 0.005$, applied during testing. Cyclic testing was performed at 2 Hz to a maximum strain of $\varepsilon_{max} = 0.8\%$ or until 150,000 cycles was reached. Apparent strains were calculated using a second gauge length measurement

conducted prior to testing. Throughout all mechanical tests, samples were immersed in a 0.9% physiological saline solution with 10 μmol/L PI to minimize tissue degradation. It is understood that testing bone dry results in an increase in Young's modulus and strength but a decrease in toughness and thus would negatively affect mechanical testing results [34].

**Microdamage Identification**

In order to label and identify initial plus preexisting microcracks from propagated microcracks, an established sequential fluorescent staining method was utilized [35-36]. Preliminary studies verified the protocol by showing no replacement of stains (Figure 2.1). Samples were stained with 0.02% Alizarin Complexone (A3882, Sigma-Aldrich) after the first mechanical test to capture preexisting damage, including damage formed *in vivo* and during sample preparation. To remove any unbound alizarin stain, samples were rinsed in deionized water for 1 hour. After cyclic testing, specimens were stained with 0.005% calcein (C-0875, Sigma-Aldrich) to label microdamage created or propagated due to cyclic compressive loading. Again, specimens were rinsed in deionized water for 1 hour to remove excess calcein stain. All specimens were gently shaken with endcaps attached in staining solutions containing 10 μmol/L PI at atmospheric pressure and at 4°C for 8 hours. Following staining in calcein solution, samples were dehydrated in a series of graded alcohols and embedded in methyl methacrylate (MMA). MMA blocks were sectioned using a precision diamond saw to create longitudinal slices 130-200 μm thick (n = 7 per age except age 77, n = 6) which were mounted onto glass slides using the non-fluorescing Eukitt's mounting medium (EM Sciences, USA).

Initial damage and cyclic load induced damage were quantified at 100X magnification with grayscale images taken under red and green epifluorescence, respectively. Microdamage types were identified according to a categorization adapted from literature [33, 37] (Figure 2.2). Microdamage propagation was assessed by a qualitative evaluation of stain intensity via the microscope and an overlapped image of the initial damage and cyclic load induced damage. Four types of microcrack progression were identified and categorized (Figure 2.3). The bone area of each slide was determined using image analysis software (AxioVs40 V4.7.1.0, Carl Zeiss Imaging Solutions GmbH) under bright field and at 40X magnification. All microdamage was quantified as damage events and normalized to each respective slide bone area. In order to avoid counting microcrack artifacts created during preparation, microdamage and bone area were valid only within a region of interest (ROI) defined as the rectangular area 500 μm from each bone edge.

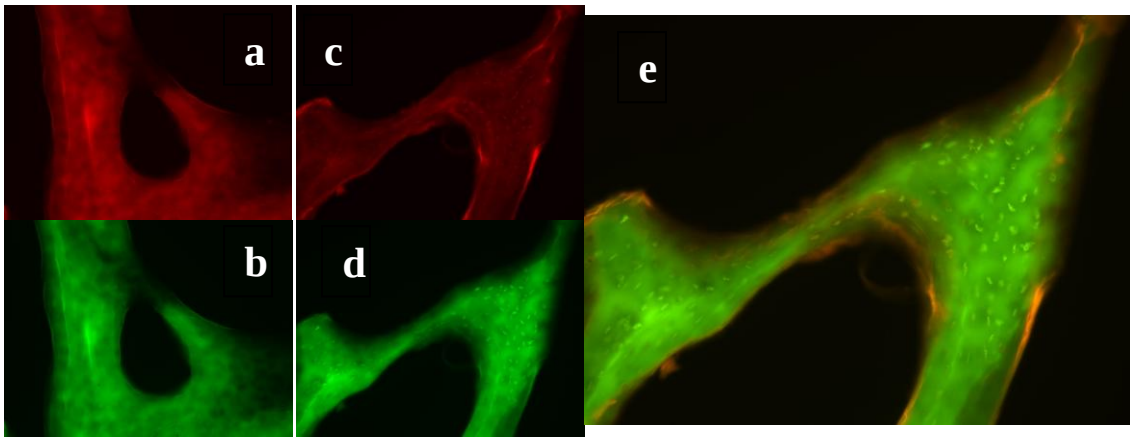


Figure 2.1: Fluorescent staining method validation. Bone autofluoresces under UV light due to the high collagen I content [38]. a & b) This autofluorescence does not interfere with microdamage identification because it fluoresces at a lower intensity. Representative image of bone stained with c) alizarin (red) and d) calcein (green). e) There is no replacement of alizarin stain by calcein stain as seen by the d) lack of bright green color in areas where c) red is bright. There is slight bleed through of calcein fluorescence when viewed under red epifluorescence as evidenced by the slight change in color from red to red-orange.

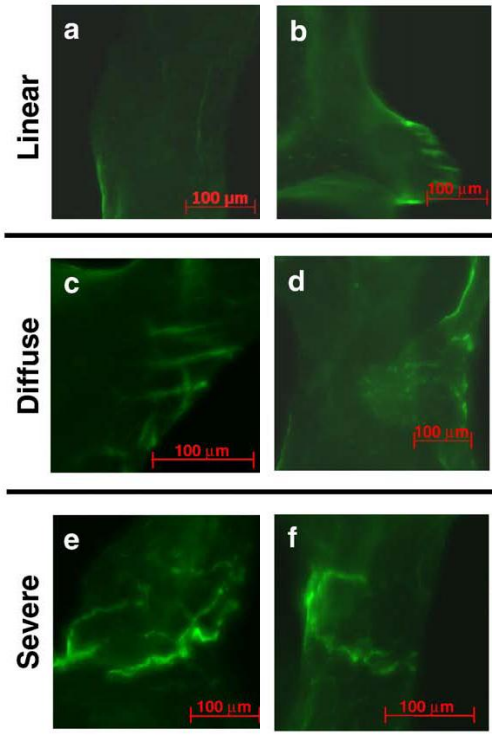


Figure 2.2: Microdamage description types. *i. Linear* damage including a) single crack and b) parallel cracks, *ii. Diffuse* (crosshatch) damage including c) equal crosshatching and d) large area distribution, *iii. Severe* damage including e) one primary crack with minor secondary cracks and f) through-thickness cracks. [37]

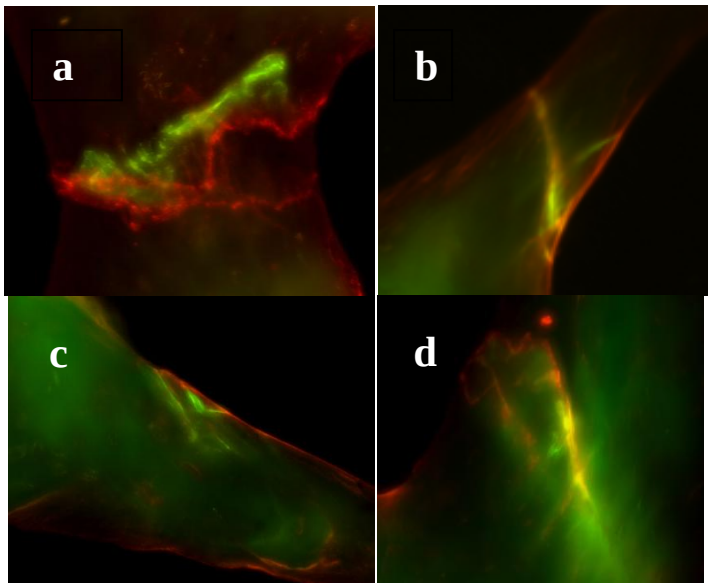


Figure 2.3: Microdamage progression classifications. Alizarin staining (red) indicates initial damage. Calcein staining (green) indicates cyclic load induced damage. a) Extension progression: microdamage that extends from existing cracks; b) Widening progression: overlapping stained cracks result in a bright yellow color that reflect a widening of initial damage; c) Surface originating progression: cyclic load induced cracks that start at surface damage and progress into trabeculae; d) Combination progression: microdamage progression that includes two or more of the other classes

### Statistics

T-tests, ANOVA analyses, and Tukey's pairwise comparisons (Minitab Inc., USA) were used to determine statistical significance for trabecular microdamage, architecture, morphology, mineralization, and mechanical properties. Significance was defined as $p < 0.05$ for all statistical tests. Microdamage comparisons were based on each slide from each donor. For the donor aged 77, an average value for the 6 slides was used as a replacement for the missing seventh slide. All data presented are in the form of mean ± standard error.

## Results

### Trabecular Architecture

Nearly all trabecular architectural parameters showed no statistical differences between groups (Figures 2.4 and 2.5). Bone volume fraction was the same between young bone (0.17 ± 0.03) and old bone (0.16 ± 0.01). Trabecular thickness in young samples (150.0 ± 29.0 μm) and old samples (137.8 ± 5.5 μm) also showed no differences. Trabecular number was greater in older bone (1.56 ± 0.03 $mm^{-1}$) than in younger bone (1.45 ±0.06 $mm^{-1}$); similarly SMI was higher in older specimens (1.57 ± 0.09) than in younger specimens (1.23 ± 0.16), but differences were not significant. Trabecular spacing was found to be greater in young bone (0.64 ± 0.02 mm) when compared to old bone (0.59 ± 0.01 mm), but this was not significant. A significantly lesser degree of anisotropy ($p = 0.03$) along with an indication towards greater connectivity density ($p = 0.07$) and greater average mineralization ($p = 0.09$) were found when comparing older samples to younger samples.

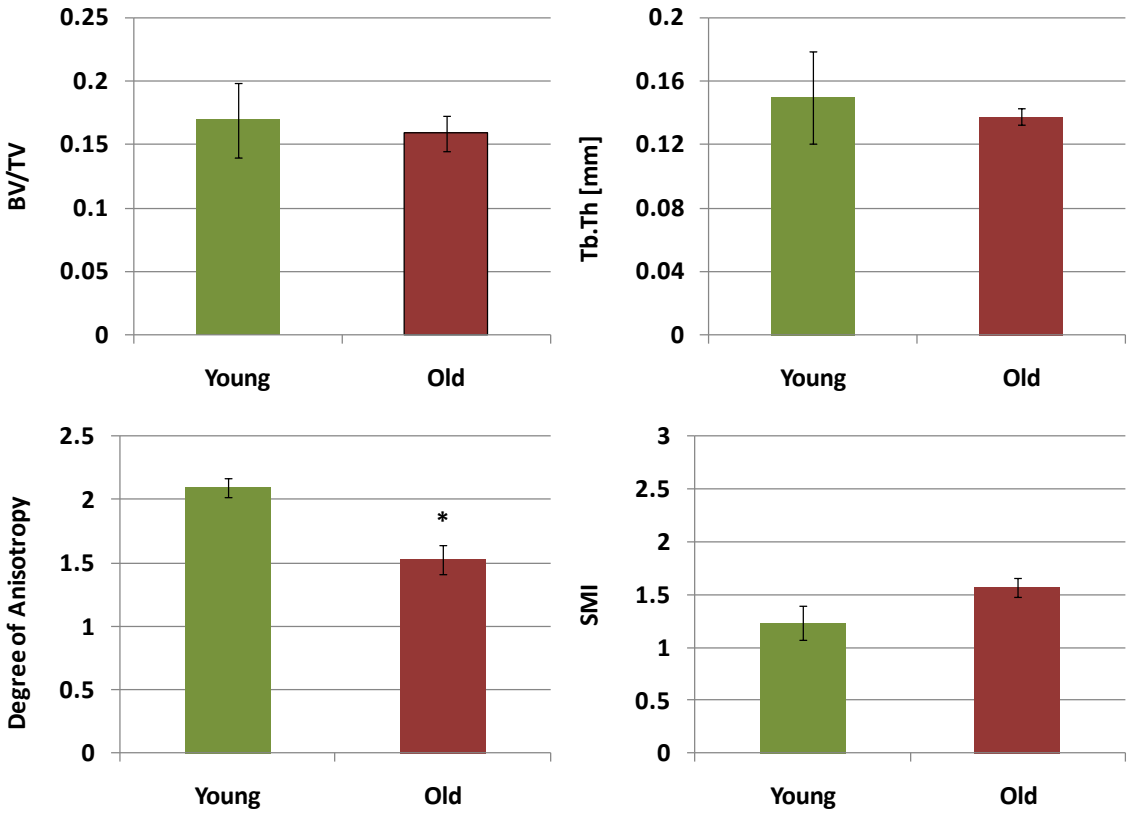


Figure 2.4: Trabecular architecture from micro-CT analysis for young (ages 29, 32, 42) and old (ages 71, 77, 82) age groups. No differences found in bone volume fraction (BV/TV), trabecular thickness (Tb.Th), and structure model index (SMI). Decreased degree of anisotropy (DA) in older bone (* indicates $p < 0.05$).

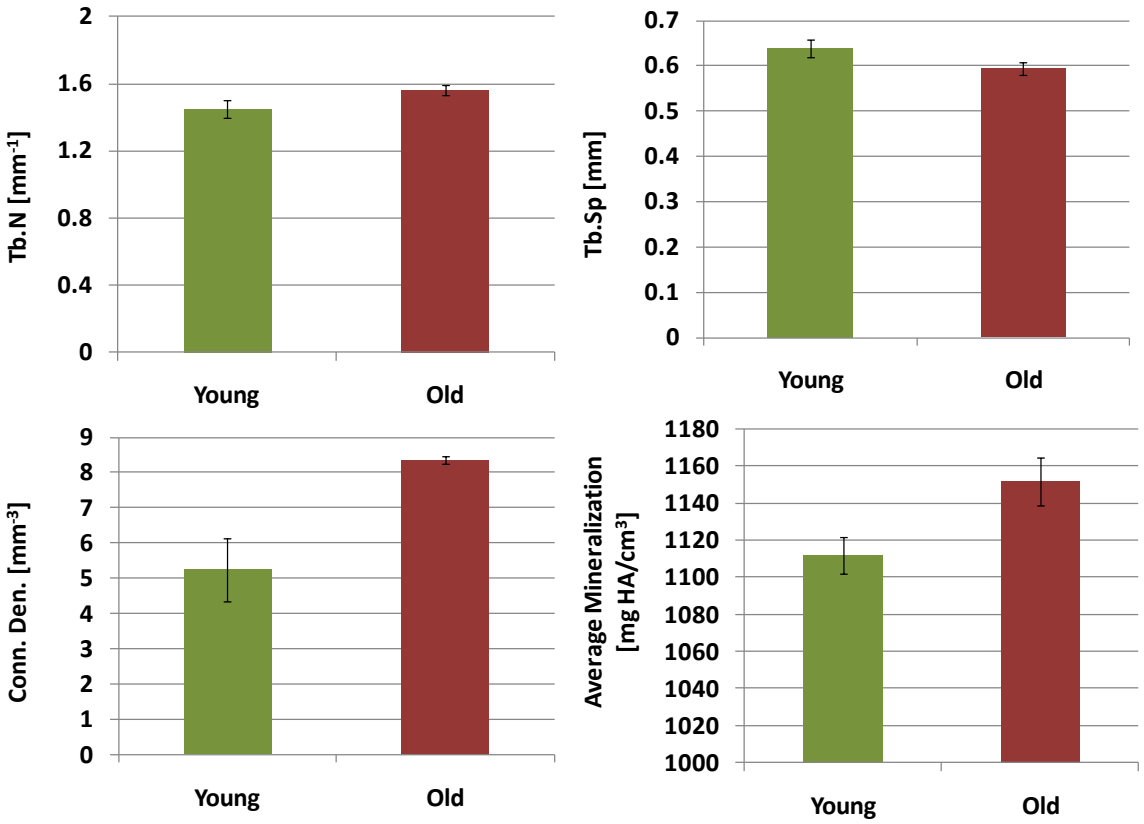


Figure 2.5: Trabecular architecture and average mineralization from micro-CT analysis for young (ages 29, 32, 42) and old (ages 71, 77, 82). No differences in trabecular number (Tb.N), trabecular spacing (Tb.Sp), connectivity density (Conn.D), and average mineralization. Non-significant higher Conn.D ($p = 0.07$) and average mineralization ($p = 0.09$).

**Mechanical Properties**

Although not significantly different ($p = 0.54$), samples from the young group (819.0 ± 234.0 MPa) were found to have a greater Young's modulus on average – measured from the first mechanical test – when compared to samples from the old group (638.8 ± 81.0 MPa). Similarly no differences were found in the initial cyclic loading modulus ($p = 0.51$) and in the associated percent modulus reduction ($p = 0.76$). Younger specimens on average lasted longer during cyclic testing (116,963 ±56,705 cycles) than older specimens (15,729 ± 14,413 cycles), but this difference was not significant ($p = 0.23$). Data can be found in Table 2.1.

Table 2.1: Mechanical testing parameters for young and old trabecular bone. Values presented as mean ± SE.

| Parameter | Young | Old | P-value (*t*-test) |
|---|---|---|---|
| Modulus (initial load, MPa) | 819.0 ± 234.0 | 638.8 ± 81.0 | 0.54 |
| Modulus (pre-cyclic load, MPa) | 410.1 ± 71.1 | 383.4 ± 25.5 | 0.76 |
| Modulus drop (%) | 44.1 ± 10.3 | 39.9 ± 5.7 | 0.68 |
| Cycles | 116963 ± 56705 | 15729 ± 14413 | 0.23 |

**Microdamage**

Two dimensional slide bone area was greater in the young group (7.50 ± 0.28 $mm^2$) than in the old group (6.70 ± 0.38 $mm^2$); however this was not statistically different ($p = 0.10$, Figure 2.6). Analysis of initial damage (young: 1.50 ± 0.18 vs. old: 2.07 ±0.15, damage events/$mm^2$) showed significant differences ($p = 0.02$), but a non-significant difference ($p = 0.05$) was found in cyclic load induced damage (young: 0.74 ± 0.10 vs. old: 1.24 ± 0.11, damage events/$mm^2$) (Figure 2.7). Both young and old bone ($p < 0.001$) had more initial damage than cyclic load induced damage.

Microdamage progression was classified into four different categories (Figure 2.3). Microdamage was found to extend from initial damage (extension propagation) either by increasing the length of cracks, by increasing the extent of cracks perpendicular to the primary crack direction, or a new crack. Cyclic loading was also found to induce widening of initial damage (widening propagation) identified by a near overlap of fluorescence resulting in a bright yellow color. Cracks also formed from areas of damage at trabecular surfaces and extended into the trabecula (surface to crack propagation). Other forms of microdamage progression were a combination of the three aforementioned types (combination propagation).

Greater incidences of total microdamage progression were found in older samples (1.18 ± 0.11 damage events/$mm^2$) when compared with younger samples (0.68 ± 0.10 damage events/$mm^2$) ($p < 0.001$) (Figure 2.8). This difference remained even after normalizing for the amount of initial damage ($p = 0.02$, Figure 2.9). No differences were found in the amount of *de novo* damage as a result of cyclic loading. All propagated damage classes were found in young and old bone with widening the most prevalent on

average and surface damage originating cracks the least prevalent in old ($p < 0.001$) and young bone ($p < 0.01$ compared to widening only) (Figure 2.10). Although there was a general increase in the amount of microcrack propagation classes except for surface originating damage, changes were only significant for combination type progression ($p = 0.04$). Assessment of these progression categories revealed no difference in the proportion of propagated damage types between age groups. An analysis of microdamage categories adapted from literature [33, 37] – linear, diffuse, and severe types (Figure 2.2) – revealed preferential crack propagation towards similar damage types (Figure 2.11) (e.g. linear to linear). This is more apparent in the older bones ($p < 0.001$) than the younger bones (only diffuse to diffuse, $p > 0.05$) when a comparison between the different possibilities was made (e.g. linear to linear, linear to diffuse, linear to severe). There was also a greater amount of severe to severe and diffuse to diffuse microdamage propagation in older bone ($p < 0.001$) when compared to younger bone.

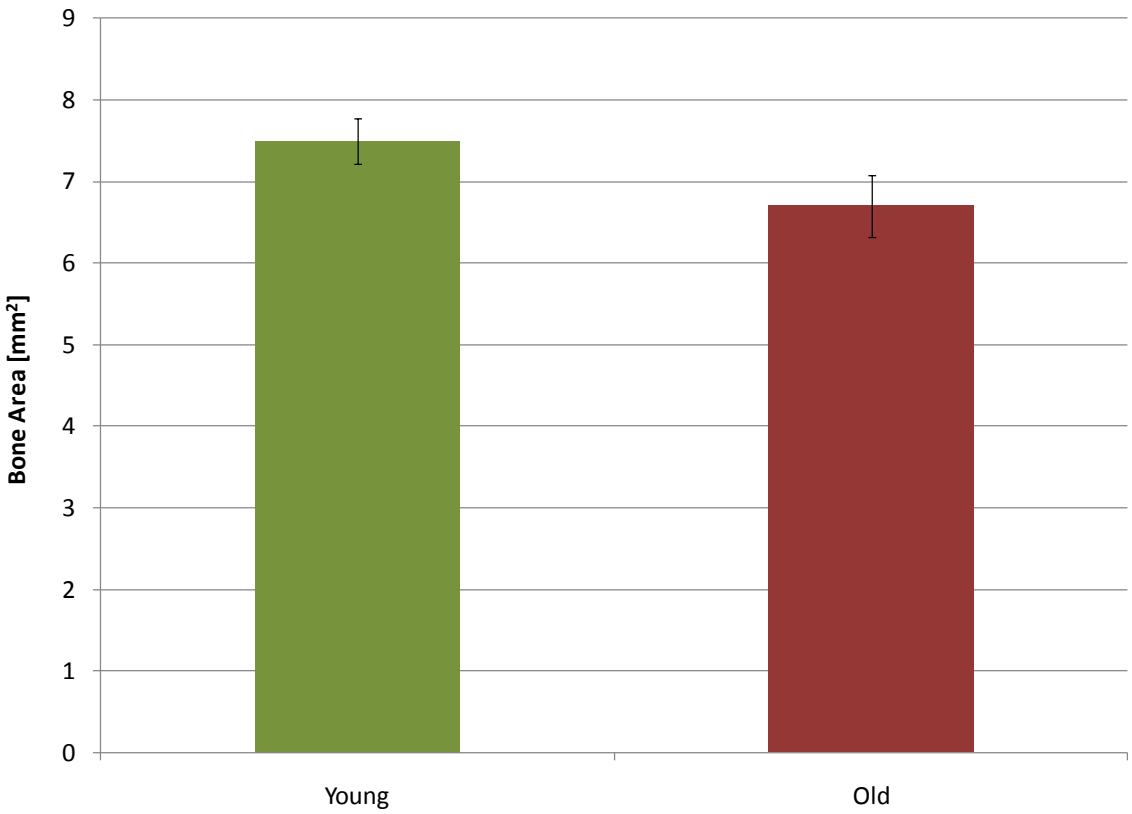


Figure 2.6: Trabecular slide bone area for young and old samples. No differences were found.

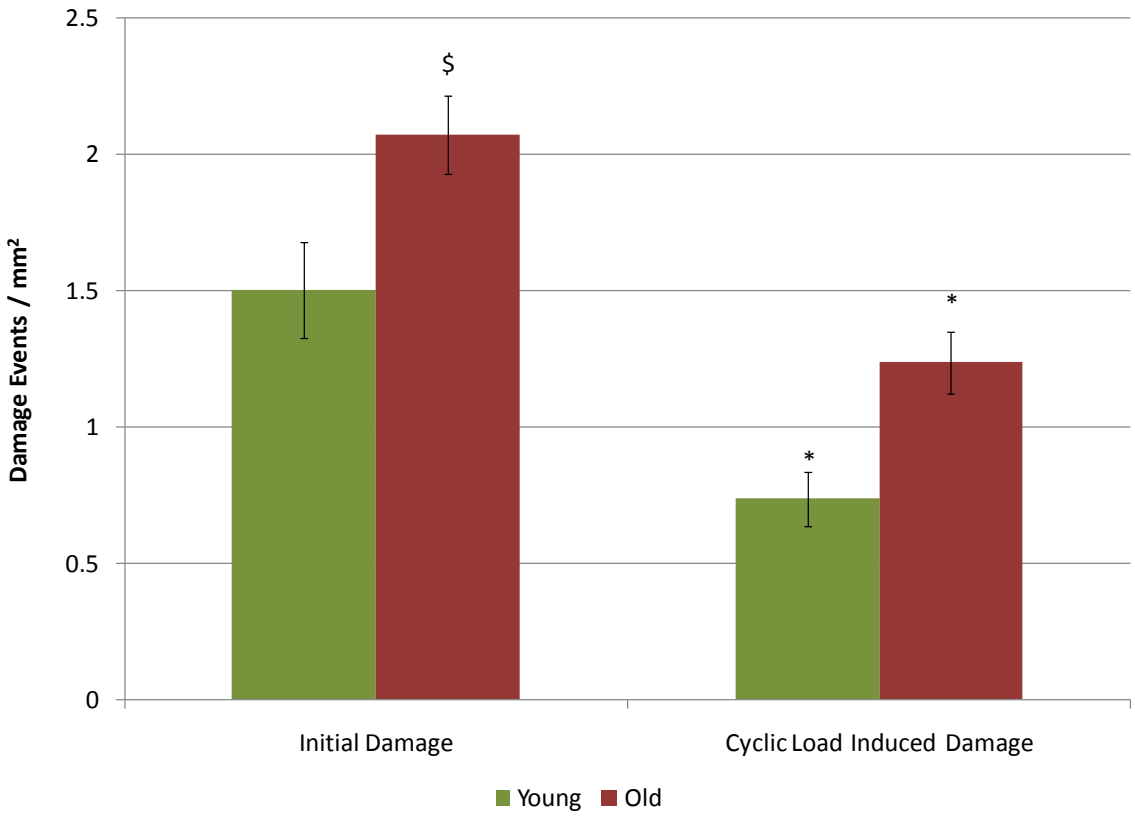


Figure 2.7: Total microdamage in young and old bone. Old bone had more initial damage than young bone ($ indicates $p < 0.05$). There was more cyclic load induced damage than initial damage in both age groups (* indicates $p < 0.001$). Old bone tended to have more cyclic induced damage than young bone ($p = 0.05$).

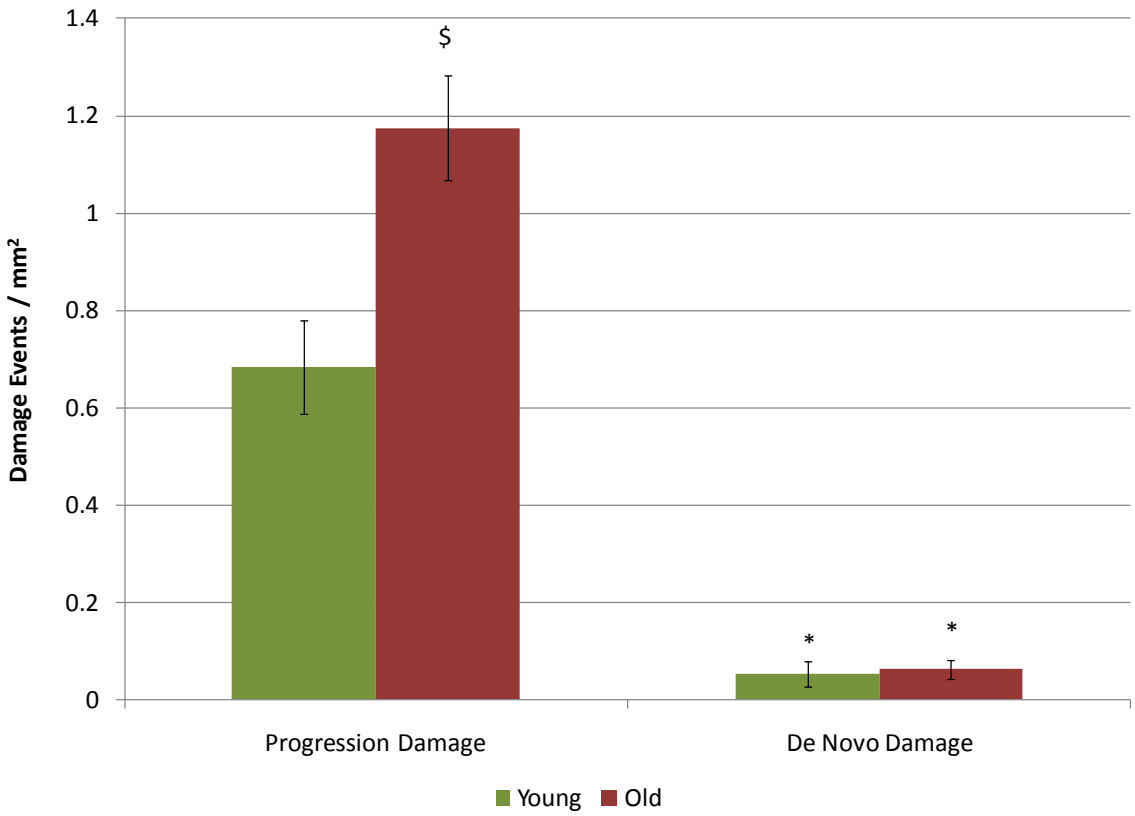


Figure 2.8: Microdamage progression and de novo damage for young and old bone. Old bone had more microdamage progression than young bone ($ indicates $p < 0.001$). Microdamage progression was greater than de novo damage in both age groups (* indicates $p < 0.001$).

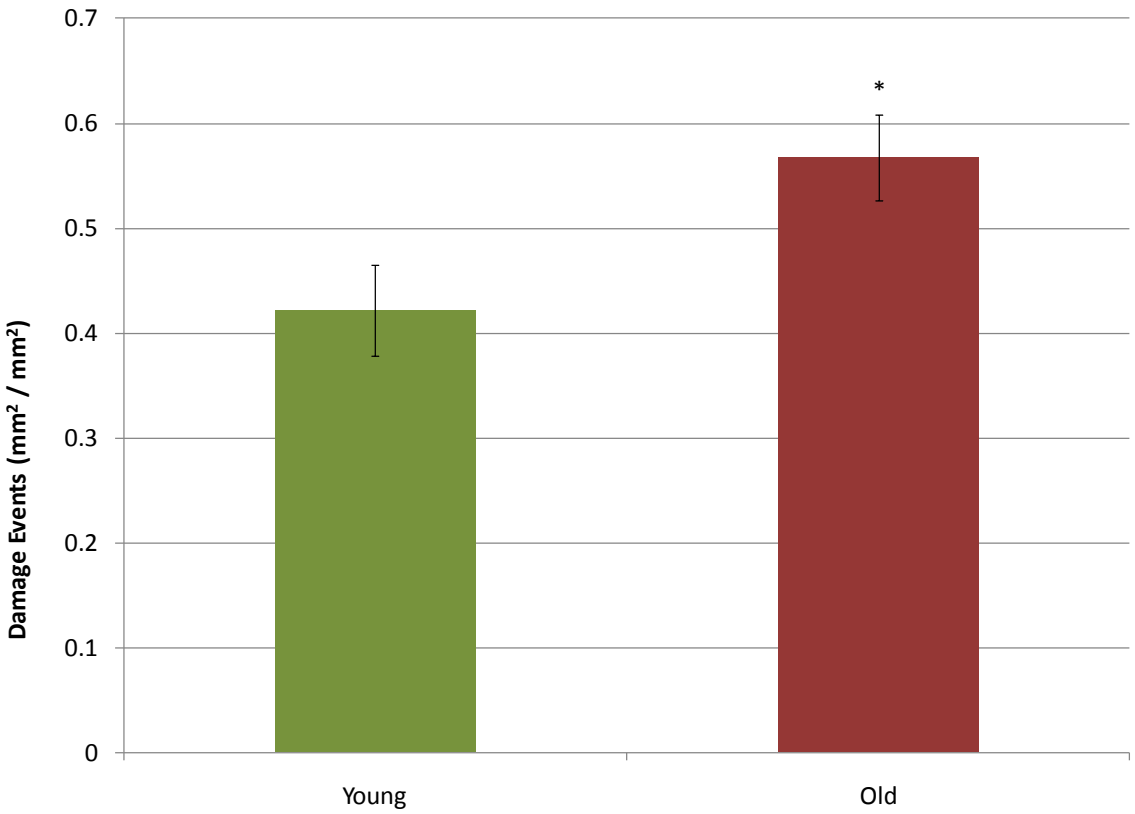


Figure 2.9: Microdamage progression normalized to initial damage. Older bone still had more progression damage after normalization (* indicates p = 0.02).

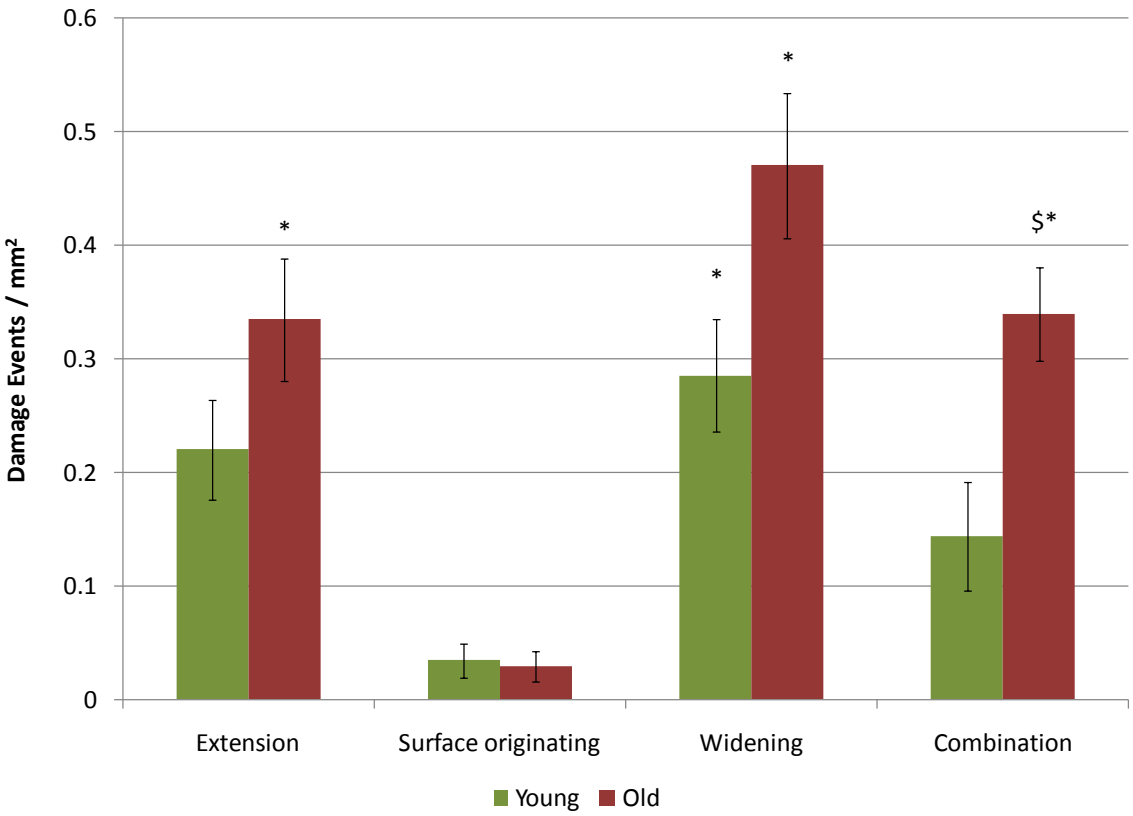


Figure 2.10: Distribution of microdamage progression classes. Surface originating class of microdamage progression was the least prevalent (* indicates $p < 0.01$ when compared to age matched surface originating class). Combination progression class was greater in old bone ($ indicates $p = 0.04$).

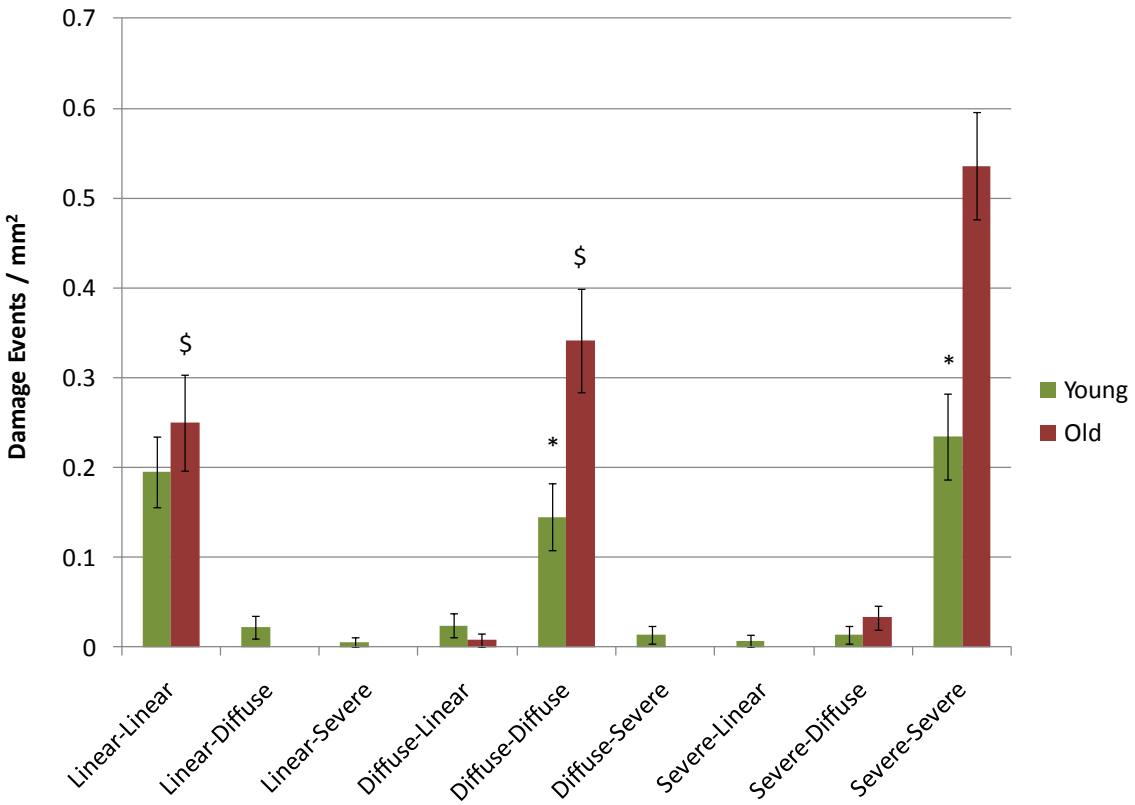


Figure 2.11: Microdamage progression characterization. Microdamage tends to propagate from and to the same microdamage types. No differences were found between young and old except with diffuse-diffuse and severe-severe sub-types where old bone had more incidences (* indicates $p < 0.001$). Within the old group, linear-linear and diffuse-diffuse sub-types occurred less than severe-severe ($ indicates $p < 0.001$).

## Discussion

Skeletal fragility is characterized by low bone mass, altered trabecular architecture, and compromised tissue matrix properties leading to increased fracture risk [21, 26]. Age-related accumulation of microdamage contributes to changes in the mechanical integrity of bone tissue, reducing apparent level mechanical properties [10, 16]. However its role in increasing fracture risk is unclear. Furthermore, studies investigating microdamage progression have mainly looked at cortical bone and have largely assumed similar damage characteristics in trabecular bone. In this study, the age-related effects on microdamage progression in trabecular bone were analyzed as a means to assess the quality of bone tissue. Microdamage was induced with an initial stress relaxation compression test followed by low stress, high cycle fatigue loading. It was found that amounts of microdamage progression occurred more in old bone, thus reflecting compromised tissue matrix properties and a reduced resistance to microcrack growth.

Although statistical analysis of mechanical testing data showed no differences, the data shows interesting results. On average the young bone exhibited a 24% greater elastic modulus than old bone, as expected. However, the elastic modulus as measured prior to cyclic loading showed similar values between age groups, thus indicating a larger modulus reduction after initial damage formation for the young bone. This implies that a greater amount of microdamage was formed in younger bone due to the first mechanical test [15, 39]. Concurrently, this reduction in modulus may reflect the low amounts of preexisting damage (damage created *in vivo*) in young bone followed by a rapid increase due to applied loads in order to dissipate local stresses and strains and prevent fracture.

Since the amounts of preexisting damage were combined with the damage formed by initial compressive loading, it is not possible to determine exactly which age group had more initial test induced damage. Despite this reduction in stiffness, young bone lasted longer on average during cyclic loading, implying a greater fatigue life compared to old bone.

Microarchitectural parameters showed expected results on average for age-related changes in BV/TV, SMI, and Tb.Th with an indication towards increase in mineralization. The discrepancies in the remaining parameters (Conn.D, Tb.N, Tb.Sp, and DA) require further discussion. An increase of SMI values towards 3 reflects more rod-like trabeculae and is associated with aging. Since the young trabecular bone is more plate-like, the changes due to aging are likely a perforation through resorption of existing trabecular plates [40-41]. With plates being remodeled into rods, the greater trabecular number and connectivity density and lower trabecular separation are easily explained by the presence of more trabecular rods. This may also explain the significantly lower degree of anisotropy in old bone. It is known that remodeling is imbalanced with age and consequently, bone resorption is not as targeted or as effective [20]. The gradual thinning of existing rods and transformation of plates to rods may have created a structure that is considerably more isotropic than it was before. However, continued inefficient remodeling would eventually remove redundant trabecular struts, presumably creating a more anisotropic structure. Another explanation may be the location the bone cores were extracted from. An effort was made to study only trabecular cores taken from the outer edges of the distal femur where trabecular bone is most dense. Even so, slight variability

in the original location of the samples may be attributed to the difference, but it is not likely.

As expected, more initial damage was present in old bone when compared to young bone. This damage includes both *in vivo* and initial test-induced microdamage and thus no conclusions can be drawn regarding preexisting damage and age. Cyclic loading resulted in less microdamage than was found for initial damage in both age groups. This result in conjunction with the greater amount of microdamage progression in old bone suggests that initiation of *de novo* microcracks does not occur to alleviate local stresses and strains. Rather, microcracks are allowed to grow as a result of applied loads. This is contrary to a study that used finite element modeling to suggest that further microdamage is formed in response to continued loading [42]. However results presented here showing microdamage progression agrees with a study conducted by Wang et al [43]. Consequently, the greater amount of microdamage progression present in old bone would indicate a compromised tissue matrix that is unable to arrest crack growth. However, it is possible that the multiple loads "saturated" the sample being tested with microdamage. This would suggest that microcracks could not form anywhere else within the trabecular core to diffuse the applied loads and thus microdamage progression was inevitable. Regardless, the results show that old bone has more microdamage progression even when normalized to the amount of initial damage, thus reflecting a poorer tissue matrix.

Further characterization of microdamage progression was conducted to determine if the different classes observed were related to aging. No differences were found between groups, but it is interesting to note that surface originating damage progression occurs very infrequently regardless of age. This may be due to the aforementioned

"saturation" of microdamage in the bone. There was also a greater amount of combination type microdamage progression in old bone versus young bone, possibly indicating a greater deleterious effect from this class of damage propagation. The results also show a preference of microdamage to progress to a similar type of microdamage (i.e. linear to linear, diffuse to diffuse, severe to severe). No known studies in trabecular bone have characterized microdamage progression in this manner.

It is important to consider the limitations of this study. The small sample size reduced the power of comparisons as reflected in the mechanical testing and micro-CT data. However the focus of this study was to investigate microdamage progression and sufficient data was available to conduct this comparison. The use of three stains to label preexisting, initial test-induced and cyclic load induced damage would have provided further information in order to characterize the behavior of microdamage progression with respect to age. A preliminary study was conducted to investigate this, but it was found that the use of three fluorochromes was not clear enough to distinguish three different damage time points. Finite element modeling has been used previously in our lab to correlate stresses and strains to microdamage initiation. This is a linear model and is not applicable to the case of microdamage progression which would require a non-linear model [44] not established within our lab.

In this aim, the age-related changes in microdamage progression were investigated as a means to assess the tissue matrix properties. It was found that old bone had more microdamage progression even when normalized to amounts of initial damage. This reflects compromised bone matrix properties in the old bone and indicates increased propensity for further damage accumulation and propagation to potential fracture.

## References


1. McDonnell, P., P.E. McHugh, and D. O'Mahoney, *Vertebral osteoporosis and trabecular bone quality.* Ann Biomed Eng, 2007. **35**(2): p. 170-89.

2. Wang, X., et al., *Age-related changes in the collagen network and toughness of bone.* Bone, 2002. **31**(1): p. 1-7.

3. Paschalis, E.P., et al., *Bone fragility and collagen cross-links.* J Bone Miner Res, 2004. **19**(12): p. 2000-4.

4. Burr, D.B., *The contribution of the organic matrix to bone's material properties.* Bone, 2002. **31**(1): p. 8-11.

5. Norman, T.L., T.M. Little, and Y.N. Yeni, *Age-related changes in porosity and mineralization and in-service damage accumulation.* J Biomech, 2008. **41**(13): p. 2868-73.

6. Dempster, D.W., *The contribution of trabecular architecture to cancellous bone quality.* J Bone Miner Res, 2000. **15**(1): p. 20-3.

7. Stauber, M. and R. Muller, *Age-related changes in trabecular bone microstructures: global and local morphometry.* Osteoporos Int, 2006. **17**(4): p. 616-26.

8. Ding, M. and I. Hvid, *Quantification of age-related changes in the structure model type and trabecular thickness of human tibial cancellous bone.* Bone, 2000. **26**(3): p. 291-5.

9. Ding, M., et al., *Age-related variations in the microstructure of human tibial cancellous bone.* J Orthop Res, 2002. **20**(3): p. 615-21.

10. Schaffler, M.B., K. Choi, and C. Milgrom, *Aging and matrix microdamage accumulation in human compact bone.* Bone, 1995. **17**(6): p. 521-25.

11. Mori, S., et al., *Trabecular bone volume and microdamage accumulation in the femoral heads of women with and without femoral neck fractures.* Bone, 1997. **21**(6): p. 521-6.

12. Fazzalari, N.L., et al., *Three-dimensional confocal images of microdamage in cancellous bone.* Bone, 1998. **23**(4): p. 373-8.

13. Fazzalari, N.L., J.S. Kuliwaba, and M.R. Forwood, *Cancellous bone microdamage in the proximal femur: influence of age and osteoarthritis on damage morphology and regional distribution.* Bone, 2002. **31**(6): p. 697-702.

14. Diab, T., et al., *Age-dependent fatigue behaviour of human cortical bone.* Eur J Morphol, 2005. **42**(1-2): p. 53-9.

15. Burr, D.B., et al., *Does microdamage accumulation affect the mechanical properties of bone?* J Biomech, 1998. **31**(4): p. 337-45.

16. Zioupos, P., *Accumulation of in-vivo fatigue microdamage and its relation to biomechanical properties in ageing human cortical bone.* J Microsc, 2001. **201**(Pt 2): p. 270-8.

17. Lu, W.W., et al., *Microfracture and changes in energy absorption to fracture of young vertebral cancellous bone following physiological fatigue loading.* Spine (Phila Pa 1976), 2004. **29**(11): p. 1196-201; discussion 1202.

18. Frost, H.M., *Presence of microscopic cracks in vivo in bone.* Henry Ford Hospital Medical Bulletin, 1960. **8**: p. 25-35.

19. Burr, D.B., *Targeted and nontargeted remodeling.* Bone, 2002. **30**(1): p. 2-4.

20. Recker, R.R., *Transmenopausal and age-related changes in bone remodeling.* J Musculoskelet Neuronal Interact, 2003. **3**(4): p. 411-2; discussion 417.

21. Turner, C.H., *Biomechanics of bone: determinants of skeletal fragility and bone quality.* Osteoporos Int, 2002. **13**(2): p. 97-104.

22. Vashishth, D., K.E. Tanner, and W. Bonfield, *Contribution, development and morphology of microcracking in cortical bone during crack propagation.* J Biomech, 2000. **33**(9): p. 1169-74.

23. Nalla, R.K., et al., *Effect of aging on the toughness of human cortical bone: evaluation by R-curves.* Bone, 2004. **35**(6): p. 1240-6.

24. O'Brien, F.J., D. Taylor, and T. Clive Lee, *The effect of bone microstructure on the initiation and growth of microcracks.* J Orthop Res, 2005. **23**(2): p. 475-80.

25. Burr, D., *Microdamage and bone strength.* Osteoporos Int, 2003. **14 Suppl 5**: p. S67-72.

26. Burr, D.B., et al., *Bone microdamage and skeletal fragility in osteoporotic and stress fractures.* J Bone Miner Res, 1997. **12**(1): p. 6-15.

27. Linde, F. and H.C. Sorensen, *The effect of different storage methods on the mechanical properties of trabecular bone.* J Biomech, 1993. **26**(10): p. 1249-52.

28. Keaveny, T.M., et al., *Differences between the tensile and compressive strengths of bovine tibial trabecular bone depend on modulus.* J Biomech, 1994. **27**(9): p. 1137-46.

29. Keaveny, T.M., et al., *Systematic and random errors in compression testing of trabecular bone.* J Orthop Res, 1997. **15**(1): p. 101-10.

30. Nagaraja, S., A.S. Lin, and R.E. Guldberg, *Age-related changes in trabecular bone microdamage initiation.* Bone, 2007. **40**(4): p. 973-80.

31. Moore, T.L. and L.J. Gibson, *Fatigue of bovine trabecular bone.* J Biomech Eng, 2003. **125**(6): p. 761-8.

32. Moore, T.L. and L.J. Gibson, *Fatigue microdamage in bovine trabecular bone.* J Biomech Eng, 2003. **125**(6): p. 769-76.

33. Arthur Moore, T.L. and L.J. Gibson, *Microdamage accumulation in bovine trabecular bone in uniaxial compression.* J Biomech Eng, 2002. **124**(1): p. 63-71.

34. Turner, C.H. and D.B. Burr, *Basic biomechanical measurements of bone: a tutorial.* Bone, 1993. **14**(4): p. 595-608.

35. Lee, T.C., et al., *Sequential labelling of microdamage in bone using chelating agents.* J Orthop Res, 2000. **18**(2): p. 322-5.

36. O'Brien, F.J., D. Taylor, and T.C. Lee, *An improved labelling technique for monitoring microcrack growth in compact bone.* J Biomech, 2002. **35**(4): p. 523-6.

37. O'Neal, J.M., et al., *One year of alendronate treatment lowers microstructural stresses associated with trabecular microdamage initiation.* Bone, 2010. **47**(2): p. 241-7.

38. Prentice, A.I., *Autofluorescence of bone tissues.* J Clin Pathol, 1967. **20**(5): p. 717-9.

39. Yeh, O.C. and T.M. Keaveny, *Relative roles of microdamage and microfracture in the mechanical behavior of trabecular bone.* J Orthop Res, 2001. **19**(6): p. 1001-7.

40. Parfitt, A.M., *Trabecular bone architecture in the pathogenesis and prevention of fracture.* Am J Med, 1987. **82**(1B): p. 68-72.

41. Parfitt, A.M., et al., *Relationships between surface, volume, and thickness of iliac trabecular bone in aging and in osteoporosis. Implications for the microanatomic and cellular mechanisms of bone loss.* J Clin Invest, 1983. **72**(4): p. 1396-409.

42. Kosmopoulos, V., C. Schizas, and T.S. Keller, *Modeling the onset and propagation of trabecular bone microdamage during low-cycle fatigue.* J Biomech, 2008. **41**(3): p. 515-22.

43. Wang, X. and G.L. Niebur, *Microdamage propagation in trabecular bone due to changes in loading mode.* J Biomech, 2006. **39**(5): p. 781-90.

44. Yang, Q.D., et al., *Fracture length scales in human cortical bone: the necessity of nonlinear fracture models.* Biomaterials, 2006. **27**(9): p. 2095-113.

# CHAPTER 3

# EFFECTS OF ANTI-RESORPTIVE AGENTS ON BIOMECHANICAL PROPERTIES AND MICRODAMAGE INITIATION IN RAT BONE

## Introduction

Osteoporosis is a disorder affecting the bone resulting in low bone mass and deterioration of bone microarchitecture leading to an increased risk and incidence of fracture [1]. Over 2 million cases of fracture costing an estimated $17 billion were predicted for 2005 [2]. These numbers are expected to increase by nearly 50% by the year 2025. There are many treatments for osteoporosis, including the use of the pharmacological therapies bisphosphonates (e.g. alendronate, ALN) and selective estrogen receptor modulators (SERMs, e.g. raloxifene, RAL). These drugs are categorized as anti-remodeling – more specifically anti-resorptive – agents due to their inhibition of the resorption of bone. This action results in increased bone mass and, clinically, reduced fracture risk [3-6]. However the similarities between the two drugs end there. In clinical trials, raloxifene (RAL) was shown to increase bone mineral density (BMD) by less than 3% in vertebrae but reduce the fracture risk by 39% [6]. Trials with alendronate (ALN) showed increases in BMD at various sites up to nearly 14% and a decrease in fracture risk of 36% [3, 5]. However the contribution of BMD to reduction in fracture risk was 4% in RAL and 17% for ALN [7-8] leaving 83-96% of the reduction

unaccounted for. This suggests differing mechanisms by which the two drugs affect the biomechanical properties of bone.

Studies in a dog model have provided insight into the variable effects of clinically relevant doses of RAL and ALN. Similar to clinical results, it was shown that ALN treatment increases bone volume fraction (BV/TV) significantly and suppresses bone turnover considerably resulting in increased microdamage accumulation [9]. The effects on mechanical properties showed increased vertebral stiffness but no material property improvements. However a study using 6 times the dose recommended clinically showed a 21% reduction in vertebral toughness [10]. This result is supported by a 3 year study showing decreased toughness with ALN treatment when compared with vehicle treated dogs [11]. On the other hand, RAL has been shown to improve vertebral strength independent of bone density, prevent microdamage accumulation, and to improve ultimate stress, modulus, and toughness in trabecular bone of the femoral neck [12-13]. A study in an ovariectomized rat model showed improvements in bone strength over vehicle treatment in the lumbar vertebrae and the femoral neck [14]. Although treatment with ALN increases bone volume considerably over treatment with RAL, the beneficial effects of RAL on material properties appears to be greater than ALN. Combining the two drugs may provide an additive effect that would provide both the structural and material improvements to bone.

A clinical study investigated this additive effect on BMD and biochemical markers of bone turnover in postmenopausal women with osteoporosis [15]. The results showed an increase in BMD with combined RAL and ALN treatment over either therapy alone in the femoral neck, but significant differences were found only with RAL in the

lumbar spine. They also found that combination treatment suppressed bone turnover more than either drug alone, possibly explaining the increase in BMD. From these results they concluded that the contributions of RAL and ALN were independent and additive.

The goal of this aim was to investigate the effects of combination treatment with RAL and ALN in a rat ovariectomized model on biomechanical properties. This included determining the structural properties and derived material properties of femurs and vertebrae to understand the apparent effects of treatment. Further study was conducted to determine the local tissue matrix properties as assessed through microdamage quantification. Secondary to this goal was to determine the effects of RAL with and without the presence of estrogen and to determine the different effects on biomechanical properties affected by RAL and by ALN. It was hypothesized that the combination treatment would provide the additive effects of RAL and ALN through improved biomechanical properties and would prevent increased microdamage accumulation. It was further hypothesized that the effects of RAL would be greater in estrogen-replete rats and that RAL would improve material properties over ALN.

## Materials and Methods

### Drug Treatment

Lumbar vertebrae and femurs from female Sprague-Dawley rats were obtained from Indiana University courtesy of Dr. David Burr. A total of ninety-six six-month-old rats were randomized into 6 experimental groups (SHAM, SHAM+RAL, OVX, OVX+RAL, OVX+ALN, OVX+RAL+ALN; n = 16/group). Rats in all groups except the sham-operated groups (SHAM) underwent bilateral ovariectomy (OVX). After a post-operative seventeen day acclimation period, the following compound administration was

delivered subcutaneously: RAL (0.5 mg/kg/day), ALN (1.0 μg/kg/day), RAL (0.5 mg/kg/day) + ALN (1.0 μg/kg/day), or daily saline vehicle (in equivalent volume to the drug treatments). The doses for RAL and ALN represent the clinical treatment dose for postmenopausal women [12, 16-17]. One rat was removed from the OVX+ALN group due to illness. Rats were euthanized 16 weeks (approximately 4 remodeling cycles) after the initiation of treatment.

**Micro-CT Imaging**

A total of 95 fresh frozen femurs from the right limb were thawed at room temperature and soft tissue was carefully removed. A section at the middiaphyseal point of each femur approximately 100 slices (about 1.6 mm) thick as identified using micro-CT (μCT 40, Scanco Medical, Bassersdorf, Switzerland) was subsequently scanned at a voxel size of 16 μm (55 kVp, 145 μA). Bone was isolated from background using a threshold applied to all samples. Using built in scanner software, the distance from the centroid to the surface of bone in tension and the cross-sectional moment of inertia (MOI) were determined. Specimens were submerged in a 0.9% physiological saline solution to prevent dehydration during imaging. After scanning, each femur was wrapped in saline soaked gauze and stored at -20°C until mechanical testing.

A total of 79 L6 vertebrae (V1) were used to study architectural and biomechanical properties and 15 L5 vertebrae (V2) were used for microdamage analysis. In group V1, all groups were considered in subsequent analyses, but in group V2, SHAM+RAL was omitted because no changes were expected in microdamage from SHAM. All L5 and L6 vertebrae were isolated and carefully cleaned of soft tissue. Posterior elements and transverse processes were removed using a bone cutter to isolate

vertebral bodies and to facilitate micro-CT scanning. To ensure parallel ends for mechanical testing [9], cranial and caudal endplates were removed using a custom made fixture and a precision diamond saw (Isomet 1000 Precision Saw, Buehler Ltd., USA). Four L6 vertebrae in group V1 (SHAM, n = 1; ALN, n = 2; OVX+RAL+ALN, n = 1) were fractured during preparation and replaced with corresponding L5 vertebrae. Samples were then scanned at a voxel size of 12 μm (55 kVp, 145 μA) in a 0.9% physiological saline and 10 μmol/L protease inhibitor (PI, E-64, Sigma Chemical) solution to minimize tissue degradation. For each vertebra, the two dimensional (2D) images obtained from micro-CT scanning were analyzed for a representative vertebral bone cross sectional area (CSA), defined as the average of the 2D CSA measured at three different positions (25, 50, and 75% of the total vertebral height) [9]. Using standard scanner software, whole vertebra (cancellous and cortical bone) fractional volume ($BV/TV_{whole}$), trabecular bone volume fraction ($BV/TV_{trab}$), and trabecular microarchitecture were obtained for a 1.2 mm region directly above the caudal growth plate. This volume of interest was isolated to avoid any errors that would be introduced by the anterior venous foramen. Trabecular architecture values included trabecular number (Tb.N, $mm^{-1}$), trabecular thickness (Tb.Th, mm), trabecular spacing (Tb.Sp, mm), connectivity density (Conn.D, $mm^{-3}$), structural model index (SMI), and mineralization (measured in mg $HA/cm^3$). The trabecular compartment was separated from the cortical shell using an adapted segmentation algorithm “dual threshold” [18].

**Mechanical Testing**

Femurs were thawed at room temperature and tested using a standard three-point bending test to failure using a servo-hydraulic mechanical testing system (858 Mini

Bionix II, MTS Corp.). The right femoral shafts were centrally loaded under displacement control at a rate of 0.6 mm/min. Custom made fixtures with rounded supports of 1.08 mm thicknesses were set to a bottom span of 19 mm. Structural, or extrinsic, properties (i.e. ultimate load, UL; stiffness, S; work to ultimate load, W) were determined from the load-displacement curve. Derived material, or intrinsic, properties (i.e. ultimate stress, $\sigma_{ult}$; elastic modulus, E; yield stress, $\sigma_{yield}$; and toughness, U) were calculated from stress and strain values determined using standard beam-bending equations for 3-point bending [19]:

$$\sigma = \frac{Lsc}{4I}$$

$$\varepsilon = \frac{12cd}{s^2}$$

Where *L* is the load, *s* is the span, *c* is the distance from the centroid to the surface of bone in tension, *I* is the moment of inertia around the axis of bending, and *d* is the displacement. One sample from the OVX group fractured prior to mechanical testing and was removed from analysis.

Group V1 vertebrae were tested under uniaxial compression to failure at a rate of 0.5 mm/min on a servo-hydraulic mechanical testing system [20]. All samples were attached to the compression platens with a minimal amount of glue to prevent slipping during testing. Structural properties (i.e. ultimate load, UL; stiffness, S; and work to failure, W) were determined from load-displacement data. Derived material properties (i.e. normalized stiffness, nS; normalized ultimate load, nUL; normalized work to failure, nW) were determined by normalizing the structural properties to vertebral geometry and $BV/TV_{whole}$ using the following equations [9, 12]:

$$nS = \frac{(S \times h/CSA)}{BV/TV_{whole}}$$

$$nUL = \frac{UL/CSA}{BV/TV_{whole}}$$

$$nW = \frac{W/(h \times CSA)}{BV/TV_{whole}}$$

Where h is the vertebral height measured using digital calipers before mechanical testing.

Immediately following micro-CT scanning, group V2 vertebrae were loaded according to a previously established uniaxial compression testing protocol [21] adapted for this study. Samples were glued to the stationary compression platen and preloaded under displacement control to ensure contact between the loading platen and the cranial surface of the vertebra. Following 3 cycles of preconditioning to 0.1% strain, specimens were loaded at 0.5% strain/s to a final strain of 1.3% and held there for 3 hours to ensure microdamage formation. Preliminary studies showed that 1.3% strain was the yield strain, but loading to this point did not incur significant amounts of trabecular fracture and thus was used. Samples were immersed in a 0.9% physiological saline and 10 μmol/L PI solution throughout mechanical testing.

**Microdamage Identification**

Only group V2 vertebrae were analyzed for the presence of microdamage using an established sequential labeling method [22-24]. The researcher was blinded to treatment groups until post-hoc analysis. Prior to mechanical testing, samples were stained with 0.02% Alizarin Complexone (A3882, Sigma-Aldrich) to label preexisting microdamage, including microcracks formed *in vivo* and during specimen preparation. After mechanical testing, vertebrae were stained with 0.005% calcein (C-0875, Sigma-

Aldrich) to label test induced microdamage. All specimens were gently shaken in staining solutions with 10 μmol/L PI at 4°C for 8 hours under atmospheric pressure. After each staining step, a 1 hour rinse in deionized water was performed to remove any excess unbound stain. After calcein labeling, vertebrae were dehydrated in a series of graded alcohols and embedded in methyl methacrylate (MMA). MMA blocks were sectioned into 100-150 μm longitudinal slices (n = 9 slides/group) using a precision diamond saw resulting in coronal slices of vertebrae and mounted onto glass slides with the non-fluorescing Eukitt's mounting medium (EM Sciences, USA).

Slides were imaged under a 10X objective utilizing fluorescence microscopy. Preexisting and test induced microcracks were quantified with grayscale images under red and green epifluorescence, respectively. Damage was categorized according to a modified microdamage identification method [24-25]. The trabecular bone area of each slide was determined using image analysis software (AxioVs40 V4.7.1.0, Carl Zeiss Imaging Solutions GmbH) under bright field and a 4X objective. Microcracks were quantified per slide as total damage events normalized to each respective slide trabecular bone area. A region of interest (ROI) 500 μm from the cranial and caudal ends and approximately 100 μm from the cortical shell was used for microdamage counting.

**Study Groups**

Experimental groups were further broken down into 3 different study groups to address different objectives during post-hoc analysis (Figure 3.1). Objective 1 (SHAM, OVX, SHAM+RAL, OVX+RAL) was to test the effects of RAL in estrogen replete versus estrogen deficient rats. Objective 2 (SHAM, OVX, OVX+RAL, OVX+ALN) was to address the beneficial effects of RAL, but not ALN, on material properties. Finally,

objective 3 (SHAM, OVX, OVX+RAL, OVX+ALN, OVX+RAL+ALN) was to determine the beneficial, if any, effects introduced by combination treatment of RAL and ALN.

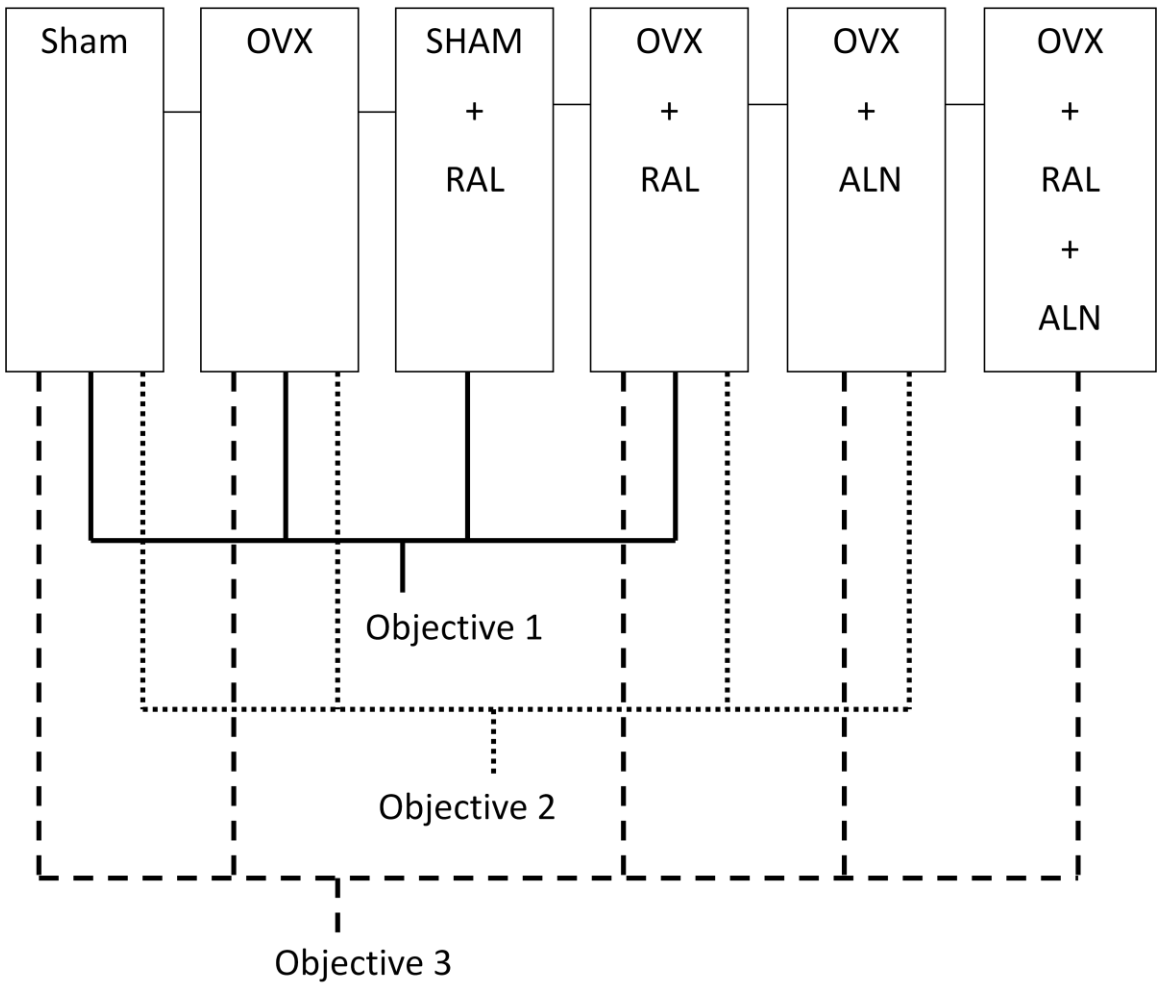


Figure 3.1: A diagram of the experimental design. a) Objective 1 compares SHAM, OVX, SHAM+RAL, and OVX+RAL to assess the hypothesis that the positive effects of RAL on bone material properties will be greater in estrogen-replete than in estrogen-deficient rats. b) Objective 2 compares SHAM, OVX, OVX+RAL, and OVX+ALN to evaluate the hypothesis that RAL will improve material properties but not ALN. c) Objective 3 compares SHAM, OVX, OVX+RAL, OVX+ALN, and OVX+RAL+ALN to determine if the combination treatment of RAL and ALN will improve both structural and material properties of bone.

### Statistics

After verification of normality using Anderson-Darling normality tests, significant differences between groups for biomechanical properties and microarchitecture were determined using one-way analysis of variance (ANOVA) tests followed by Fisher's pairwise comparisons. Microdamage comparisons were made using regression analysis with Tukey's pairwise comparisons. If the normality criterion was not met, the Kruskal-Wallis test was utilized to look for significance followed by Mann-Whitney pairwise comparisons. Significance was defined as $p < 0.05$ for all significance tests. Statistics presented are in the form of mean ± standard error. All statistics were run using MINITAB software (Minitab, Inc., USA).

## Results

### Objective 1: RAL with and without Estrogen

Femoral volumetric BMD (vBMD) was different between SHAM and OVX+RAL only ($p < 0.01$) (Table 3.1). No differences were found in MOI between groups ($p > 0.50$). Only ultimate load contained differences between groups ($p < 0.01$): SHAM v OVX, SHAM+RAL v OVX+RAL, SHAM v OVX+RAL, SHAM+RAL v OVX. Stiffness and energy to failure comparisons between groups were not significant ($p > 0.05$). Ultimate stress was significantly higher in the SHAM group than OVX ($p = 0.01$), SHAM+RAL ($p = 0.04$), and OVX+RAL ($p < 0.01$). No differences were found in toughness or elastic modulus ($p > 0.05$).

In the vertebrae, ovariectomy compromised BV/TV, trabecular architecture, and mineralization values when compared with other groups ($p < 0.001$) (Table 3.2). SHAM values were not found to be different from SHAM+RAL values ($p > 0.05$) for any

parameter. However OVX+RAL was significantly different from SHAM+RAL across all values except mineralization ($p < 0.001$). OVX+RAL returned mineralization levels to SHAM levels ($p < 0.001$).

Treatment with RAL in vertebrae did not significantly improve any structural or derived material properties when compared with controls ($p > 0.05$) (Table 3.3). The SHAM group had greater ultimate load and stiffness than the OVX group ($p < 0.05$).

Table 3.1: Femur micro-CT results and mechanical properties for Objective 1. Values presented as mean ± SE. vBMD, volumetric bone mineral density; MOI, moment of inertia. ([A] significantly different from SHAM, [B] significantly different from OVX, [C] significantly different from SHAM+RAL)

| | SHAM | OVX | SHAM+RAL | OVX+RAL | P-value |
|---|---|---|---|---|---|
| vBMD (mg HA/cm$^3$) | 1458.7 ± 8.0 | 1456.3 ± 11.4 | 1454. 4 ± 16.7 | 1447.7 ± 13.0$^A$ | < 0.01 |
| MOI (mm$^4$) | 6.37 ± 0.19 | 6.59 ± 0.22 | 6.63 ± 0.21 | 6.27 ± 0.20 | 0.54 |
| Ultimate Load (N) | 137 ± 3 | 130 ± 2$^A$ | 138 ± 2$^B$ | 128 ± 3$^{A,C}$ | < 0.01 |
| Stiffness (N/mm) | 456 ± 12 | 444 ± 7 | 452 ± 14 | 418 ± 11 | 0.07 |
| Energy to Failure (mJ) | 56.6 ± 2.5 | 47.7 ± 2.7 | 56.2 ± 2.9 | 52.6 ± 2.0 | 0.06 |
| Ultimate Stress (MPa) | 178 ± 2 | 167 ± 3$^A$ | 173 ± 2$^A$ | 169 ± 2$^A$ | < 0.05 |
| Modulus (GPa) | 10.31 ± 0.31 | 9.74 ± 0.27 | 9.81 ± 0.28 | 9.61 ± 0.26 | 0.31 |
| Toughness (MPa) | 4.23 ± 0.21 | 3.59 ± 0.20 | 4.02 ± 0.17 | 4.02 ± 0.15 | 0.09 |

Table 3.2: Trabecular architecture of the vertebrae assessed by micro-CT for Objective 1. Values presented as mean ± SE. BV/TV, bone volume fraction; Tb.Th, trabecular thickness; Tb.N, trabecular number; Tb.Sp, trabecular separation; Conn.D, connectivity density; SMI, structure model index. ($^{A}$ significantly different from SHAM, $^{B}$ significantly different from OVX, $^{C}$ significantly different from SHAM+RAL).

| | SHAM | OVX | SHAM+RAL | OVX+RAL | P-value |
|---|---|---|---|---|---|
| BV/TV | 0.476 ± 0.010 | 0.300 ± 0.006$^{A}$ | 0.457 ± 0.013$^{B}$ | 0.402 ± 0.008$^{A,B,C}$ | < 0.001 |
| Tb.Th (mm) | 0.090 ± 0.001 | 0.074 ± 0.001$^{A}$ | 0.088 ± 0.002$^{B}$ | 0.083 ± 0.001$^{A,B,C}$ | < 0.001 |
| Tb.N ($mm^{-1}$) | 5.50 ± 0.07 | 4.31 ± 0.07$^{A}$ | 5.39 ± 0.11$^{B}$ | 4.97 ± 0.09$^{A,B,C}$ | < 0.001 |
| Tb.Sp (mm) | 0.163 ± 0.003 | 0.223 ± 0.004$^{A}$ | 0.166 ± 0.004$^{B}$ | 0.186 ± 0.004$^{A,B,C}$ | < 0.001 |
| Conn.D ($mm^{-3}$) | 57.1 ± 2.2 | 82.6 ± 3.3$^{A}$ | 62.4 ± 2.5$^{B}$ | 70.5 ± 3.2$^{A,B,C}$ | < 0.001 |
| SMI | -2.31 ± 0.16 | -0.22 ± 0.06$^{A}$ | -2.02 ± 0.16$^{B}$ | -1.41 ± 0.09$^{A,B,C}$ | < 0.001 |
| Mineralization (mg HA/$cm^{3}$) | 1233.8 ± 2.8 | 1219.5 ± 3.8$^{A}$ | 1236.2 ± 2.3$^{B}$ | 1230.1 ± 2.0$^{B}$ | < 0.001 |

Table 3.3: Vertebrae mechanical properties for Objective 1. Values presented as mean ± SE. nUL, normalized ultimate load; nS, normalized stiffness; nW, normalized work to failure. ($^{A}$ significantly different from SHAM, $^{B}$ significantly different from OVX)

| | SHAM | OVX | SHAM+RAL | OVX+RAL | P-value |
|---|---|---|---|---|---|
| Ultimate Load (N) | 340 ± 25 | 249 ± 17$^{A}$ | 325 ± 28$^{B}$ | 264 ± 17$^{A}$ | 0.01 |
| Stiffness (N/mm) | 5247 ± 602 | 3582 ± 387$^{A}$ | 4956 ± 526$^{B}$ | 3622 ± 330$^{A}$ | 0.02 |
| Work to failure (mJ) | 17.3 ± 1.7 | 14.7 ± 1.1 | 17.1 ± 1.9 | 18.5 ± 1.9 | 0.44 |
| nUL (MPa) | 69.1 ± 4.4 | 68.2 ± 4.0 | 65.5 ± 4.9 | 61.8 ± 4.1 | 0.64 |
| nS (GPa) | 5.68 ± 0.59 | 5.61 ± 0.57 | 5.40 ± 0.49 | 4.69 ± 0.43 | 0.29 |
| nW (MPa) | 0.661 ± 0.067 | 0.694 ± 0.042 | 0.637 ± 0.061 | 0.791 ± 0.085 | 0.49 |

**Objective 2: RAL versus ALN**

No differences were found in femoral vBMD or MOI across groups ($p > 0.05$) (Table 3.4). Biomechanical testing of the femur showed increased ultimate load in OVX+ALN when compared to OVX and OVX+RAL ($p < 0.01$). Treatment with ALN resulted in greater stiffness values than RAL ($p = 0.03$), but no groups were different from OVX. OVX+RAL stiffness values were significantly lower than SHAM values ($p = 0.03$). SHAM and OVX+ALN had greater energy to failure values than OVX ($p = 0.02$), but OVX+RAL did not. SHAM ultimate stress was greater than OVX and OVX+RAL ($p = 0.01$). No differences were found in toughness or modulus ($p > 0.05$).

Vertebral BV/TV was improved over OVX with ALN and RAL ($p < 0.001$), but the treatments were not different from each other ($p > 0.05$) and were significantly less than SHAM ($p < 0.001$) (Table 3.5). Both treatment groups had significantly different Conn.D than SHAM ($p < 0.001$) but only treatment with RAL produced different values from OVX ($p < 0.001$). All other trabecular architecture values saw similar differences as with BV/TV where both treatments improved microarchitecture from OVX but not enough to reach SHAM values ($p < 0.001$). Both OVX+RAL and OVX+ALN groups had greater mineralization than OVX ($p < 0.01$).

Vertebral mechanical tests showed no improvements with ALN or RAL treatment ($p > 0.05$) (Table 3.6). Ultimate load and stiffness were decreased with OVX compared to SHAM ($p < 0.05$), but no differences were found in derived material properties.

Table 3.4: Femur micro-CT results and mechanical properties for Objective 2. Values presented as mean ± SE. vBMD, volumetric bone mineral density; MOI, moment of inertia. ([A] significantly different from SHAM, [B] significantly different from OVX, [C] significantly different from OVX+RAL)

| | SHAM | OVX | OVX+RAL | OVX+ALN | P-value |
|---|---|---|---|---|---|
| vBMD (mg HA/cm$^3$) | 1458.7 ± 8.0 | 1456.3 ± 11.4 | 1447.7 ± 13.0 | 1450.7 ± 4.6 | 0.05 |
| MOI (mm$^4$) | 6.37 ± 0.19 | 6.59 ± 0.22 | 6.27 ± 0.20 | 6.75 ± 0.26 | 0.40 |
| Ultimate Load (N) | 137 ± 3 | 130 ± 2[A] | 128 ± 3[A] | 140 ± 2[B,C] | < 0.01 |
| Stiffness (N/mm) | 456 ± 12 | 444 ± 7 | 418 ± 11[A] | 459 ± 12[C] | 0.03 |
| Energy to Failure (mJ) | 56.6 ± 2.5 | 47.7 ± 2.7[A] | 52.6 ± 2.0 | 57.6 ± 2.1[B] | 0.02 |
| Ultimate Stress (MPa) | 178 ± 2 | 167 ± 3[A] | 169 ± 2[A] | 173 ± 3 | 0.01 |
| Modulus (GPa) | 10.31 ± 0.31 | 9.74 ± 0.27 | 9.61 ± 0.26 | 9.88 ± 0.40 | 0.40 |
| Toughness (MPa) | 4.23 ± 0.21 | 3.59 ± 0.20 | 4.02 ± 0.15 | 4.12 ± 0.14 | 0.06 |

Table 3.5: Trabecular architecture of the vertebrae assessed by micro-CT for Objective 2. Values presented as mean ± SE. BV/TV, bone volume fraction; Tb.Th, trabecular thickness; Tb.N, trabecular number; Tb.Sp, trabecular separation; Conn.D, connectivity density; SMI, structure model index. ([A] significantly different from SHAM, [B] significantly different from OVX)

| | SHAM | OVX | OVX+RAL | OVX+ALN | P-value |
|---|---|---|---|---|---|
| BV/TV | 0.476 ± 0.010 | 0.300 ± 0.006[A] | 0.402 ± 0.008[A,B] | 0.395 ± 0.008[A,B] | < 0.001 |
| Tb.Th (mm) | 0.090 ± 0.001 | 0.074 ± 0.001[A] | 0.083 ± 0.001[A,B] | 0.080 ± 0.001[A,B] | < 0.001 |
| Tb.N ($mm^{-1}$) | 5.50 ± 0.07 | 4.31 ± 0.07[A] | 4.97 ± 0.09[A,B] | 5.16 ± 0.04[A,B] | < 0.001 |
| Tb.Sp (mm) | 0.163 ± 0.003 | 0.223 ± 0.004[A] | 0.186 ± 0.004[A,B] | 0.178 ± 0.002[A,B] | < 0.001 |
| Conn.D ($mm^{-3}$) | 57.1 ± 2.2 | 82.6 ± 3.3[A] | 70.5 ± 3.2[A,B] | 79.2 ± 3.9[A] | < 0.001 |
| SMI | -2.31 ± 0.16 | -0.22 ± 0.06[A] | -1.41 ± 0.09[A,B] | -1.19 ± 0.09[A,B] | < 0.001 |
| Mineralization (mg HA/$cm^3$) | 1233.8 ± 2.8 | 1219.5 ± 3.8[A] | 1230.1 ± 2.0[B] | 1231.7 ± 3.6[B] | < 0.01 |

Table 3.6: Vertebrae mechanical properties for Objective 2. Values presented as mean ± SE. nUL, normalized ultimate load; nS, normalized stiffness; nW, normalized work to failure. ($^{A}$ significantly different from SHAM).

| | SHAM | OVX | OVX+RAL | OVX+ALN | P-value |
|---|---|---|---|---|---|
| Ultimate Load (N) | 340 ± 25 | 249 ± 17$^{A}$ | 264 ± 17$^{A}$ | 287 ± 14 | < 0.01 |
| Stiffness (N/mm) | 5247 ± 602 | 3582 ± 387$^{A}$ | 3622 ± 330$^{A}$ | 3699 ± 406$^{A}$ | 0.03 |
| Work to failure (mJ) | 17.3 ± 1.7 | 14.7 ± 1.1 | 18.5 ± 1.9 | 16.9 ± 1.5 | 0.69 |
| nUL (MPa) | 69.1 ± 4.4 | 68.2 ± 4.0 | 61.8 ± 4.1 | 68.1 ± 3.5 | 0.69 |
| nS (GPa) | 5.68 ± 0.59 | 5.61 ± 0.57 | 4.69 ± 0.43 | 5.02 ± 0.58 | 0.60 |
| nW (MPa) | 0.661 ± 0.067 | 0.694 ± 0.042 | 0.791 ± 0.085 | 0.709 ± 0.076 | 0.64 |

**Objective 3: RAL and ALN Combination Treatment**

Femoral vBMD and MOI were not different between groups ($p > 0.05$) (Table 3.7). Ultimate load and stiffness values were not significantly different between OVX+RAL+ALN and OVX+RAL ($p > 0.05$), but OVX+ALN ultimate load ($p < 0.01$) and stiffness ($p = 0.02$) values were higher than the other treatment groups. SHAM ultimate load was higher than with RAL treatment ($p < 0.01$), and SHAM stiffness was greater than RAL and combination treatment ($p = 0.02$). Only treatment with ALN resulted in different values from OVX ($p < 0.01$) for ultimate load. Both SHAM and OVX+ALN groups had greater energy to failure than OVX ($p = 0.03$). No differences were found in material properties ($p > 0.05$).

In the vertebra, combination treatment improved BV/TV over ALN and RAL alone but not to SHAM levels ($p < 0.001$) (Figure 3.2). Both RAL and RAL+ALN treatment reduce Conn.D significantly from OVX values ($p < 0.001$), but only RAL+ALN treatment was different from ALN treatment results ($p < 0.001$) (Figure 3.3). Similar improvements with the OVX+RAL+ALN group were seen in SMI values ($p < 0.001$) except OVX+ALN was also different from OVX ($p < 0.001$). Combination treatment improved Tb.N and Tb.Sp more than RAL alone ($p < 0.001$) and nearly to SHAM levels. No treatment differences were found with Tb.Th. SHAM and all treatment groups had greater mineralization than OVX ($p < 0.05$) (Figure 3.4).

RAL+ALN treatment improved ultimate load over OVX and nearly to SHAM levels ($p < 0.01$) whereas RAL and ALN treatment alone resulted in ultimate loads significantly less than SHAM ($p < 0.01$) (Figure 3.5). Similarly, OVX+RAL and

OVX+ALN stiffness values were less than SHAM ($p < 0.05$). No differences in derived material properties were found (Table 3.8).

No differences were found for preexisting or test-induced microdamage in vertebrae between groups ($p > 0.10$) (Figure 3.6). Differences were found in the OVX and OVX+RAL groups in the comparisons of linear damage with diffuse damage ($p = 0.01$) and linear damage with severe damage ($p < 0.001$) (Figure 3.7).

Table 3.7: Femur micro-CT results and mechanical properties for Objective 3. Values presented as mean ± SE. vBMD, volumetric bone mineral density; MOI, moment of inertia. ([A] significantly different from SHAM, [B] significantly different from OVX, [C] significantly different from OVX+RAL, [D] significantly different from OVX+ALN)

| | SHAM | OVX | OVX+RAL | OVX+ALN | OVX+RAL+ALN | P-value |
|---|---|---|---|---|---|---|
| vBMD (mg HA/cm$^3$) | 1458.7 ± 8.0 | 1456.3 ± 11.4 | 1447.7 ± 13.0 | 1450.7 ± 4.6 | 1453.4 ± 3.1 | 0.11 |
| MOI (mm$^4$) | 6.37 ± 0.19 | 6.59 ± 0.22 | 6.27 ± 0.20 | 6.75 ± 0.26 | 6.40 ± 0.18 | 0.51 |
| Ultimate Load (N) | 137 ± 3 | 130 ± 2 | 128 ± 3[A] | 140 ± 2[B,C] | 131 ± 3[D] | < 0.01 |
| Stiffness (N/mm) | 456 ± 12 | 444 ± 7 | 418 ± 11[A] | 459 ± 12[C] | 425 ± 11[A,D] | 0.02 |
| Energy to Failure (mJ) | 56.6 ± 2.5 | 47.7 ± 2.7[A] | 52.6 ± 2.0 | 57.6 ± 2.1[B] | 52.8 ± 2.2 | 0.03 |
| Ultimate Stress (MPa) | 178 ± 2 | 167 ± 3 | 169 ± 2 | 173 ± 3 | 171 ± 3 | 0.06 |
| Modulus (GPa) | 10.31 ± 0.31 | 9.74 ± 0.27 | 9.61 ± 0.26 | 9.88 ± 0.40 | 9.55 ± 0.28 | 0.40 |
| Toughness (MPa) | 4.23 ± 0.21 | 3.59 ± 0.20 | 4.02 ± 0.15 | 4.12 ± 0.14 | 4.01 ± 0.14 | 0.09 |

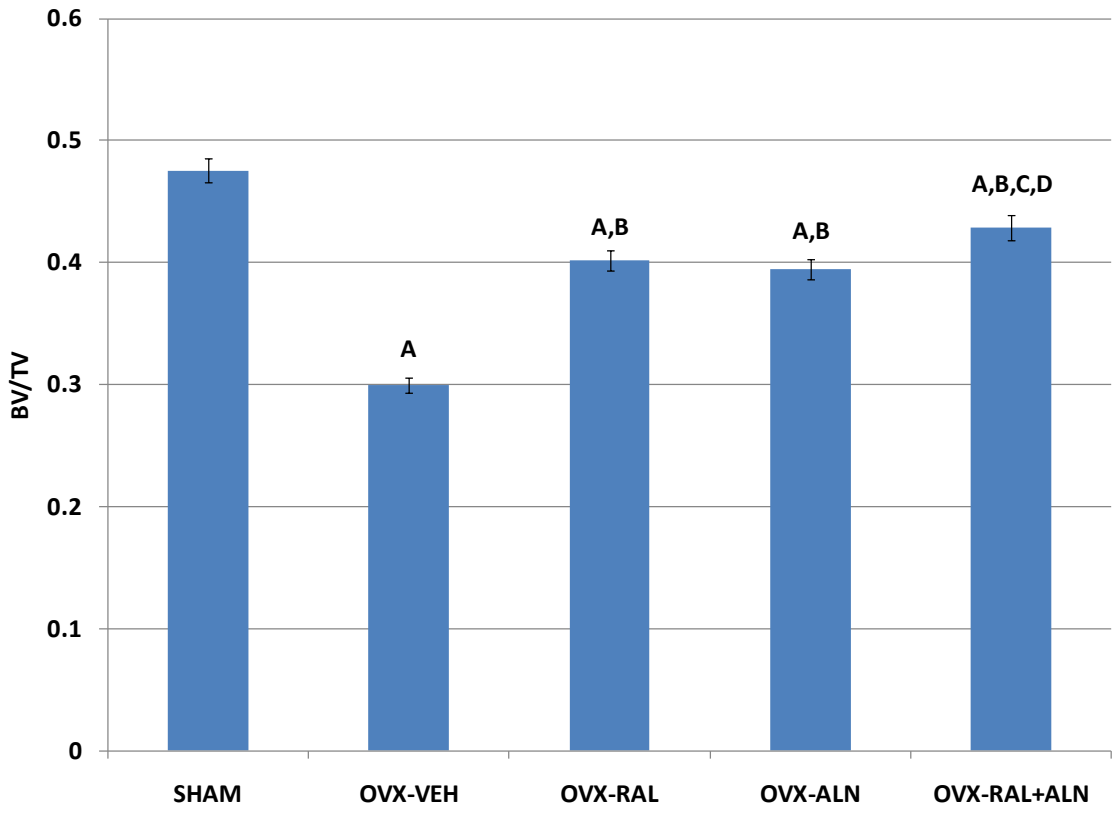


Figure 3.2: Vertebral trabecular bone volume fraction (BV/TV) for Objective 3. (A, significantly different from SHAM; B, significantly different from OVX; C, significantly different from OVX+RAL; D, significantly different from OVX+ALN). $p < 0.001$

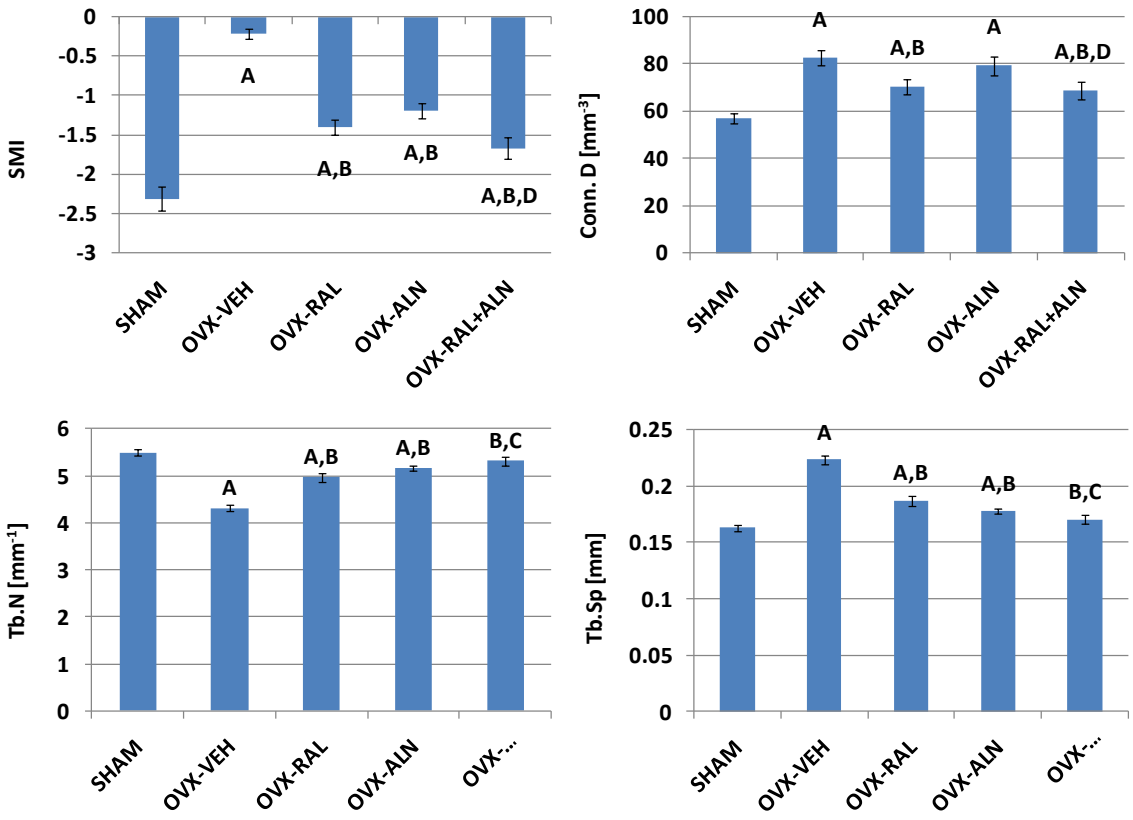


Figure 3.3: Vertebral trabecular architecture for Objective 3. (A, significantly different from SHAM; B, significantly different from OVX; C, significantly different from OVX+RAL; D, significantly different from OVX+ALN). $p < 0.001$

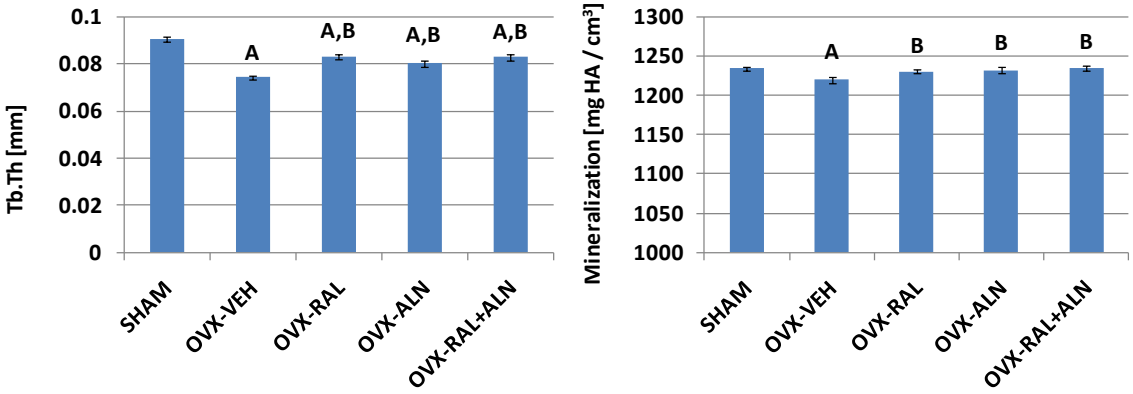


Figure 3.4: Vertebral trabecular thickness (Tb.Th, $p < 0.001$) and mineralization ($p \leq 0.01$) for Objective 3. (A, significantly different from SHAM; B, significantly different from OVX).

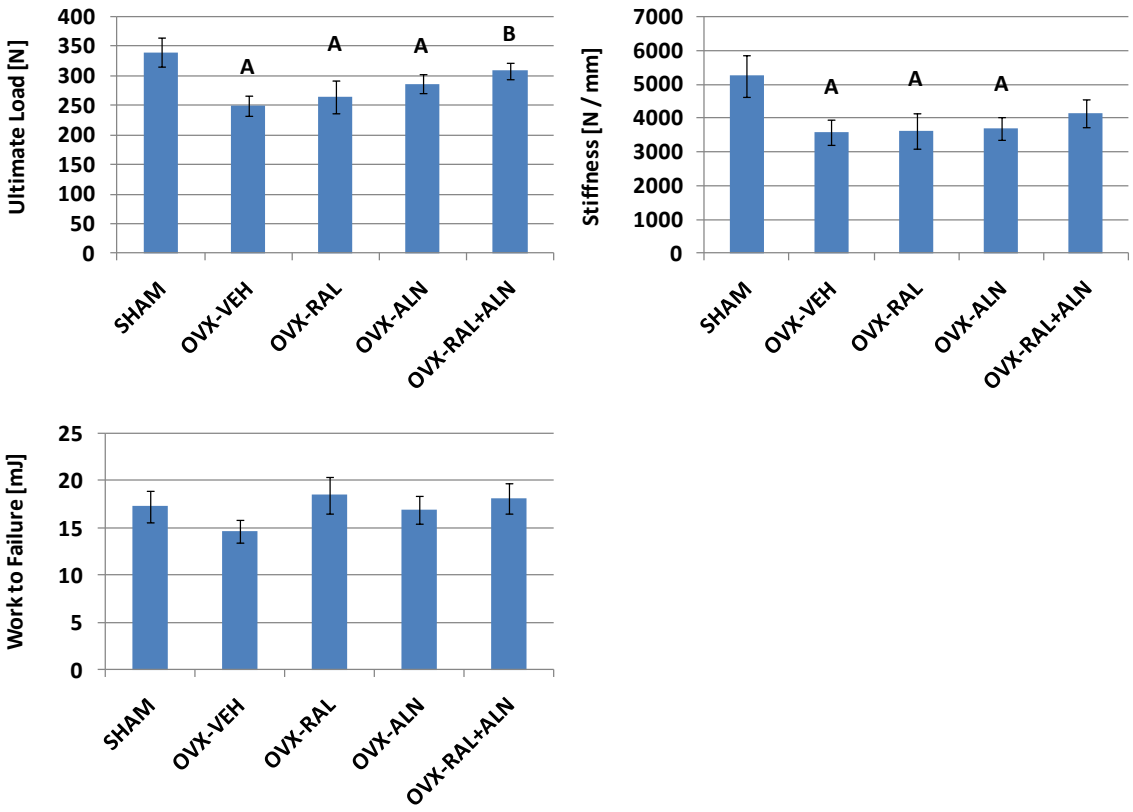


Figure 3.5: Structural (extrinsic) properties of vertebrae for Objective 3. (A, significantly different from SHAM; B, significantly different from OVX). Ultimate Load, $p < 0.01$; Stiffness, $p = 0.04$.

Table 3.8: Vertebrae material (intrinsic) properties for Objective 3. Values presented as mean ± SE. nUL, normalized ultimate load; nS, normalized stiffness; nW, normalized work to failure.

| | SHAM | OVX | SHAM+RAL | OVX+RAL | OVX+ALN | OVX+RAL+ALN | P-value |
|---|---|---|---|---|---|---|---|
| nUL (MPa) | 69.1 ± 4.4 | 68.2 ± 4.0 | 65.5 ± 4.9 | 61.8 ± 4.1 | 68.1 ± 3.5 | 67.1 ± 2.2 | 0.69 |
| nS (GPa) | 5.68 ± 0.59 | 5.61 ± 0.57 | 5.40 ± 0.49 | 4.69 ± 0.43 | 5.02 ± 0.58 | 4.92 ± 0.48 | 0.60 |
| nW (MPa) | 0.661 ± 0.067 | 0.694 ± 0.042 | 0.637 ± 0.061 | 0.791 ± 0.085 | 0.709 ± 0.076 | 0.7420.082 | 0.64 |

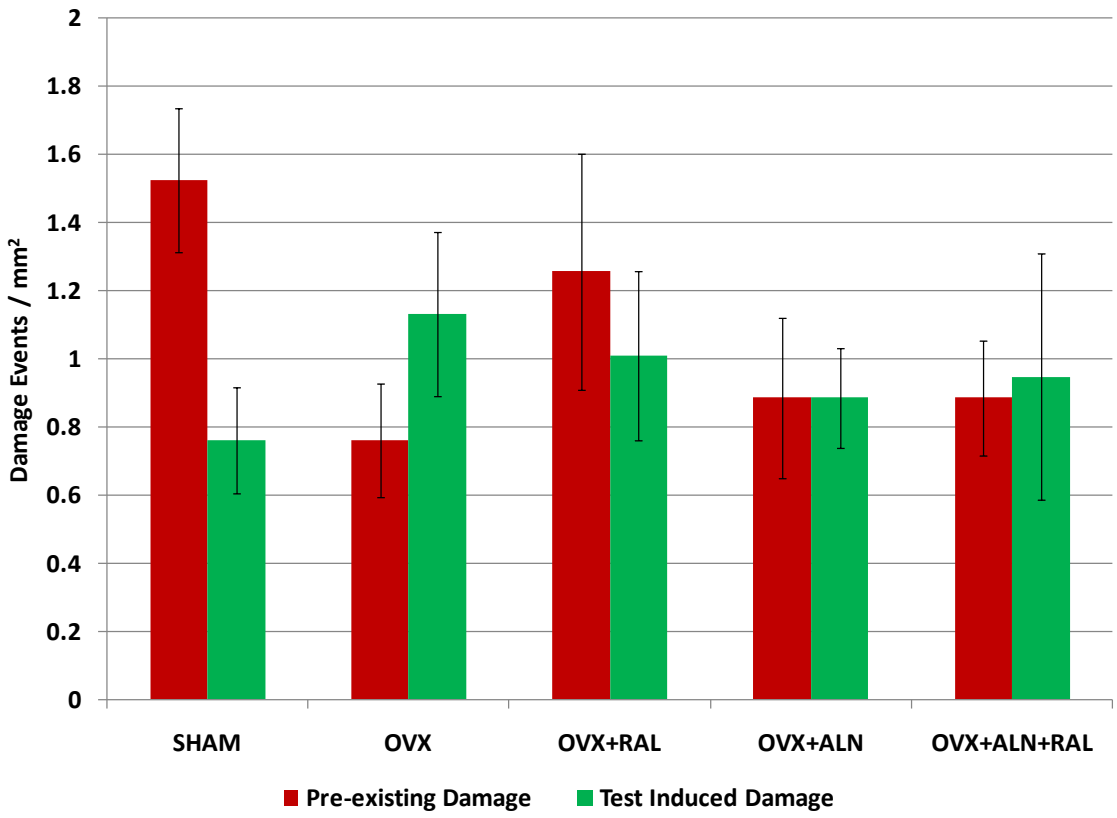


Figure 3.6: Preexisting and test-induced damage in vertebrae for Objective 3. No significant differences were found.

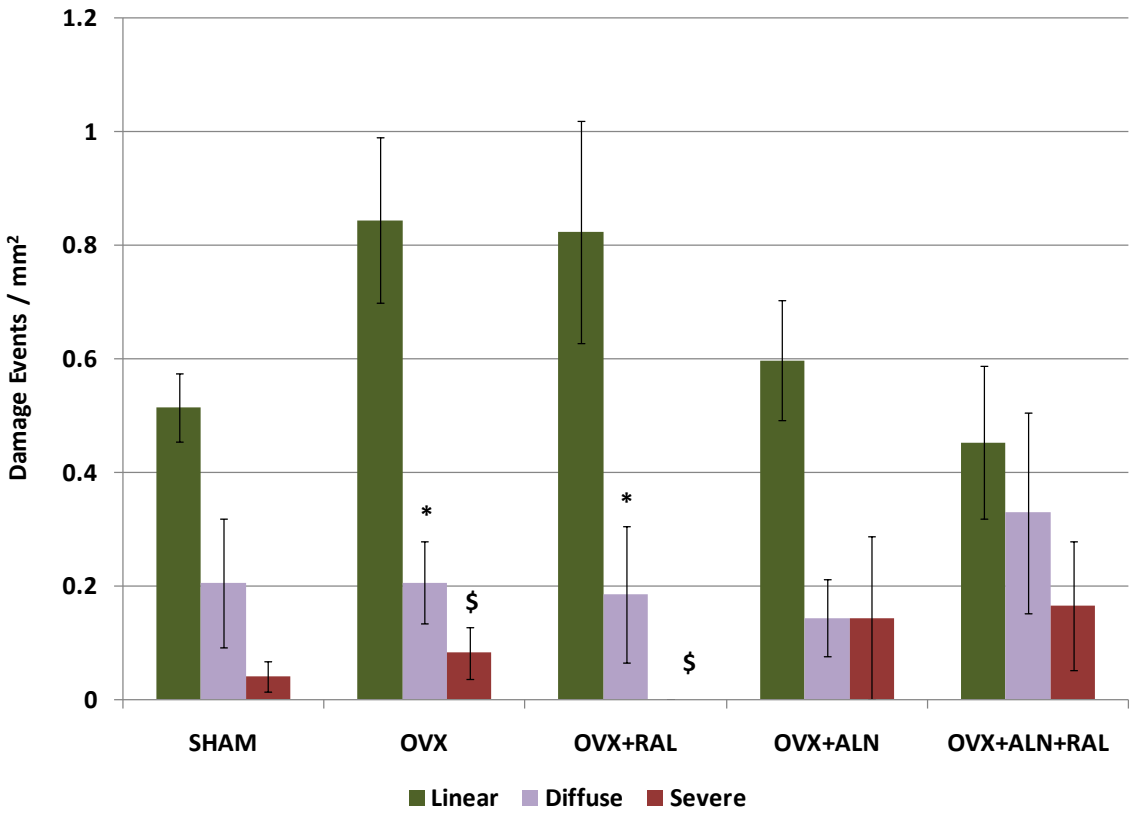


Figure 3.7: Microdamage types within test-induced damage. Significant differences between linear and diffuse damage (* indicates p = 0.01 when compared to linear damage in same group) and between linear and severe damage ($ indicates p < 0.001 when compared with linear damage in same group) within OVX and OVX+RAL groups. Lack of this difference in combination treatment (OVX+RAL+ALN) implies some resistance to the formation of the deleterious linear damage in relation to the amounts of diffuse and severe damage.

## Discussion

Osteoporotic fractures are a considerable health concern. With an increasing aging population due to longer life expectancies, the incidences and costs associated with fractures can only be expected to increase [2]. Current therapies, such as the bisphosphonate alendronate (ALN) and the selective estrogen receptor modulator (SERM) raloxifene (RAL), are used clinically to inhibit the natural bone remodeling process and increase bone mineral density (BMD). Clinical studies have shown that RAL treatment increases BMD to a lesser degree than ALN but reduces fracture risk by a comparable amount [3-6]. Animal studies using ALN showed that ALN improves BMD and consequently structural properties but diminishes the material properties of bone [9-11]. Similar studies evaluating RAL showed that this drug improves material properties with modest improvements to bone volume fraction [12-13]. Based on a clinical study evaluating combination treatment of RAL and ALN [15], it seems reasonable that the combination of these two drugs would both improve bone volume, structural properties, and material properties without the associated drawbacks of each drug. Thus the aim of this study was to determine the effects of RAL+ALN combination treatment on the bone biomechanical properties through mechanical tests and the bone matrix properties through quantification of microdamage. The results showed a significant increase in bone volume and improvement of trabecular architecture that coincided with a higher ultimate load with combination treatment that neither treatment alone could produce. Treatment with RAL and ALN together also resulted in a decrease of linear microdamage relative to diffuse and severe damage. These findings suggest that a combination treatment of RAL and ALN may be more effective in preventing fractures.

While treatment with RAL in estrogen replete and deficient rats showed no differences in biomechanical properties, improvements were found in BV/TV and trabecular architecture between OVX and OVX+RAL but no differences between SHAM and SHAM+RAL. This indicates positive effects by RAL in the absence of estrogen and lack thereof with the presence of estrogen. However these results are not in agreement with other studies that have shown increased vertebral strength in an OVX rat model [14] and increased material properties in a non-ovariectomized dog model [13]. One reason may be the treatment duration. In the rat study, RAL administration occurred over a 6 month period. However, the dosage was also 6 times the amount in the current study and the rats were 10 to 11 weeks in age at ovariectomy compared to 24 weeks for the current study. Compared to the study in dogs, the treatment duration was nearly equivalent as far as remodeling cycles but the difference is in the mean tissue age. Aging tissue matrix results in increased microdamage accumulation and decreased mechanical properties [26-27].

Treatment with ALN improved vertebral trabecular architecture and BV/TV with no differences with RAL treatment. No effects on material properties were found, but ALN treatment had a positive effect on structural properties in the femur, i.e. ultimate load, stiffness, and energy to failure. Although beneficial, the lack of effects in the vertebrae for both structural and derived material properties limits the applicability of the positive results on femurs to reduction of more clinically relevant fracture risk. In addition, the issues of treatment duration and mean tissue age prevent comparisons with reports of clinical fractures of the femoral shaft [28].

In agreement with the results from Johnell et al [15], treatment with RAL and ALN in combination resulted in significantly greater BV/TV in the vertebra than both ALN and RAL alone. This was associated with an improvement in the vertebral ultimate load that was not different from SHAM. Improvements in trabecular architecture were also better than either drug alone produced. Specifically, RAL+ALN resulted in better Conn.D and SMI values than ALN while improving Tb.N and Tb.Sp to a greater degree than RAL. Tb.Th values were not different between treatment groups. Looking solely at the SHAM and OVX groups, an explanation for the resulting values in microarchitectural parameters can be provided. A negative SMI value indicates a dense trabecular structure with closed cavities in them, resembling Swiss cheese [29-32]. As the SMI value becomes less negative (tending towards zero and positive values) the structure begins to have more open cavities as a result of resorption. This results in a decrease in BV/TV as bone is resorbed, an increase in Conn.D as more connections are "created", and a decrease in Tb.Th as plates are thinned. Trabecular separation increases as a consequence of closed cavities opening up and joining. Loss of trabecular struts due to this process then produces the loss in Tb.N. Thus, the less negative the SMI and associated changes reflects negative changes on the trabecular architecture as seen when comparing SHAM and OVX.

The lack of microdamage formation both *in vivo* and *in vitro* generally agrees with literature. One study found no differences in microdamage accumulation *in vivo* but a reduction in bone toughness of the ribs was determined [33]. No differences were found in microdamage in preexisting damage or test-induced damage at 1.0 mg/kg/day of ALN treatment in canine femoral trabeculae [24]. An increase in test induced damage was

found in the control group but not in ALN treated groups. However another study found that microdamage accumulates in the vertebrae of dogs with ALN treatment, peaking early in the administration of the drug [11]. RAL treatment did not result in increased amounts of microdamage in the literature and thus agrees with the results presented here [12]. It should be noted that linear microdamage, considered to be the most destructive type due to its propensity to propagate to catastrophic fracture [34-35], was most prevalent in OVX and OVX+RAL groups compared to diffuse and severe types of damage. While the crack lengths were not measured in this study, Allen et al found that treatment with RAL resulted in fewer but longer microcracks compared to the more abundant shorter cracks in bisphosphonate treatment [12]. The results presented here regarding the role of microdamage, especially damage morphology, with anti-resorptive treatment in an OVX rat model show promising results and warrant further investigations.

This study had a few important limitations. First, the derived material properties presented here do not reflect the true material properties of the bone. These calculations are an estimation of the bone material properties and cannot adequately account for the different factors involved with assessing bone quality. Second, when investigating microdamage formation in the rat vertebrae, certain considerations need to be taken into account. Mainly, the contributions of the cortical shell and trabecular bone and their combined contributions to bearing load contribute to the formation of microdamage.

It is important to take into account not just the trabecular architecture but the cortical shell morphology as well [36-37]. It is understood that the cortical shell serves to carry loads in the event that trabeculae fracture, but it is interesting to note that the trabecular

bone carries most of the load and that the capacity of the cortical shell to bear loads is due in part to the trabeculae connected to it [38-39]. In fact, trabecular microfracture will occur before whole bone fracture, i.e. macrofracture of the cortical shell [40]. Thus, the inclusion of finite element modeling coupled with a modified mechanical testing protocol would allow improved characterization of both the whole vertebra and the role of microdamage formation within the trabecula in apparent properties. Third, the microdamage quantification was limited by a small sample size which may have contributed to decreased power and sensitivity during analysis.

In this aim, the effects of RAL and ALN as a combination therapy on biomechanical properties and microdamage formation were investigated. It was found that combination treatment improved the vertebral ultimate load, BV/TV, and trabecular architecture better than either RAL or ALN alone did. In addition, OVX rats saw a greater amount of linear microdamage relative to diffuse and severe damage whereas OVX+RAL+ALN rats did not, suggesting potential changes on the tissue matrix properties that help prevent the formation of linear microdamage. Furthermore, the treatment effects of RAL and ALN alone did not show positive effects in the biomechanical properties of the vertebrae. Despite this, the additive effects of the two drugs were able to improve the extrinsic properties of the vertebrae and potentially the integrity of the tissue matrix, indicating a potential use of combination therapy using RAL and ALN in treating osteoporosis and reducing fracture risk.

## References


1. Cole, Z.A., E.M. Dennison, and C. Cooper, *Osteoporosis epidemiology update.* Curr Rheumatol Rep, 2008. 10(2): p. 92-6.

2. Burge, R., et al., *Incidence and economic burden of osteoporosis-related fractures in the United States, 2005-2025.* J Bone Miner Res, 2007. 22(3): p. 465-75.

3. Cummings, S.R., et al., *Effect of alendronate on risk of fracture in women with low bone density but without vertebral fractures: results from the Fracture Intervention Trial.* JAMA, 1998. 280(24): p. 2077-82.

4. Boivin, G.Y., et al., *Alendronate increases bone strength by increasing the mean degree of mineralization of bone tissue in osteoporotic women.* Bone, 2000. 27(5): p. 687-94.

5. Bone, H.G., et al., *Ten years' experience with alendronate for osteoporosis in postmenopausal women.* N Engl J Med, 2004. 350(12): p. 1189-99.

6. Delmas, P.D., et al., *Efficacy of raloxifene on vertebral fracture risk reduction in postmenopausal women with osteoporosis: four-year results from a randomized clinical trial.* J Clin Endocrinol Metab, 2002. 87(8): p. 3609-17.

7. Sarkar, S., et al., *Relationships between bone mineral density and incident vertebral fracture risk with raloxifene therapy.* J Bone Miner Res, 2002. 17(1): p. 1-10.

8. Riggs, B.L. and L.J. Melton, 3rd, *Bone turnover matters: the raloxifene treatment paradox of dramatic decreases in vertebral fractures without commensurate increases in bone density.* J Bone Miner Res, 2002. 17(1): p. 11-4.

9. Allen, M.R., et al., *Alterations in canine vertebral bone turnover, microdamage accumulation, and biomechanical properties following 1-year treatment with clinical treatment doses of risedronate or alendronate.* Bone, 2006. 39(4): p. 872-9.

10. Mashiba, T., et al., *Effects of suppressed bone turnover by bisphosphonates on microdamage accumulation and biomechanical properties in clinically relevant skeletal sites in beagles.* Bone, 2001. 28(5): p. 524-31.

11. Allen, M.R. and D.B. Burr, *Three years of alendronate treatment results in similar levels of vertebral microdamage as after one year of treatment.* J Bone Miner Res, 2007. 22(11): p. 1759-65.

12. Allen, M.R., et al., *Raloxifene enhances vertebral mechanical properties independent of bone density.* Bone, 2006. 39(5): p. 1130-5.

13. Allen, M.R., et al., *Raloxifene enhances material-level mechanical properties of femoral cortical and trabecular bone.* Endocrinology, 2007. 148(8): p. 3908-13.

14. Turner, C.H., M. Sato, and H.U. Bryant, *Raloxifene preserves bone strength and bone mass in ovariectomized rats.* Endocrinology, 1994. 135(5): p. 2001-5.

15. Johnell, O., et al., *Additive effects of raloxifene and alendronate on bone density and biochemical markers of bone remodeling in postmenopausal women with osteoporosis.* J Clin Endocrinol Metab, 2002. 87(3): p. 985-92.

16. Iwata, K., et al., *Bisphosphonates suppress periosteal osteoblast activity independently of resorption in rat femur and tibia.* Bone, 2006. 39(5): p. 1053-8.

17. Fuchs, R.K., R.J. Phipps, and D.B. Burr, *Recovery of trabecular and cortical bone turnover after discontinuation of risedronate and alendronate therapy in ovariectomized rats.* J Bone Miner Res, 2008. 23(10): p. 1689-97.

18. Buie, H.R., et al., *Automatic segmentation of cortical and trabecular compartments based on a dual threshold technique for in vivo micro-CT bone analysis.* Bone, 2007. 41(4): p. 505-15.

19. Turner, C.H. and D.B. Burr, *Basic biomechanical measurements of bone: a tutorial.* Bone, 1993. 14(4): p. 595-608.

20. Reinwald, S., et al., *Skeletal changes associated with the onset of type 2 diabetes in the ZDF and ZDSD rodent models.* Am J Physiol Endocrinol Metab, 2009. 296(4): p. E765-74.

21. Nagaraja, S., A.S. Lin, and R.E. Guldberg, *Age-related changes in trabecular bone microdamage initiation.* Bone, 2007. 40(4): p. 973-80.

22. Lee, T.C., et al., *Sequential labelling of microdamage in bone using chelating agents.* J Orthop Res, 2000. 18(2): p. 322-5.

23. O'Brien, F.J., D. Taylor, and T.C. Lee, *An improved labelling technique for monitoring microcrack growth in compact bone.* J Biomech, 2002. 35(4): p. 523-6.

24. O'Neal, J.M., et al., *One year of alendronate treatment lowers microstructural stresses associated with trabecular microdamage initiation.* Bone, 2010. 47(2): p. 241-7.

25. Arthur Moore, T.L. and L.J. Gibson, *Microdamage accumulation in bovine trabecular bone in uniaxial compression.* J Biomech Eng, 2002. 124(1): p. 63-71.

26. Wang, X., et al., *Age-related changes in the collagen network and toughness of bone.* Bone, 2002. 31(1): p. 1-7.

27. Schaffler, M.B., K. Choi, and C. Milgrom, *Aging and matrix microdamage accumulation in human compact bone.* Bone, 1995. 17(6): p. 521-25.

28. Burr, D.B., et al., *Effects of 1 to 3 years' treatment with alendronate on mechanical properties of the femoral shaft in a canine model: implications for subtrochanteric femoral fracture risk.* J Orthop Res, 2009. 27(10): p. 1288-92.

29. Kinney, J.H., et al., *Three-dimensional morphometry of the L6 vertebra in the ovariectomized rat model of osteoporosis: biomechanical implications.* J Bone Miner Res, 2000. 15(10): p. 1981-91.

30. Issever, A.S., et al., *A micro-computed tomography study of the trabecular bone structure in the femoral head.* J Musculoskelet Neuronal Interact, 2003. 3(2): p. 176-84.

31. Gasser, J.A., et al., *Noninvasive monitoring of changes in structural cancellous bone parameters with a novel prototype micro-CT.* J Bone Miner Metab, 2005. 23 Suppl: p. 90-6.

32. Mastbergen, S.C., et al., *The groove model of osteoarthritis applied to the ovine fetlock joint.* Osteoarthritis Cartilage, 2008. 16(8): p. 919-28.

33. Allen, M.R., S. Reinwald, and D.B. Burr, *Alendronate reduces bone toughness of ribs without significantly increasing microdamage accumulation in dogs following 3 years of daily treatment.* Calcif Tissue Int, 2008. 82(5): p. 354-60.

34. Burr, D.B., et al., *Does microdamage accumulation affect the mechanical properties of bone?* J Biomech, 1998. 31(4): p. 337-45.

35. Diab, T., et al., *Age-related change in the damage morphology of human cortical bone and its role in bone fragility.* Bone, 2006. 38(3): p. 427-31.

36. Roux, J.P., et al., *Contribution of trabecular and cortical components to biomechanical behavior of human vertebrae: an ex vivo study.* J Bone Miner Res, 2010. 25(2): p. 356-61.

37. Andresen, R., H.J. Werner, and H.C. Schober, *Contribution of the cortical shell of vertebrae to mechanical behaviour of the lumbar vertebrae with implications for predicting fracture risk.* Br J Radiol, 1998. 71(847): p. 759-65.

38. Forwood, M.R. and D. Vashishth, *Translational aspects of bone quality--vertebral fractures, cortical shell, microdamage and glycation: a tribute to Pierre D. Delmas.* Osteoporos Int, 2009. 20 Suppl 3: p. S247-53.

39. Eswaran, S.K., et al., *The micro-mechanics of cortical shell removal in the human vertebral body.* Computer Methods in Applied Mechanics and Engineering, 2007. 196(31-32): p. 3025-3032.

40. Kummari, S.R., et al., *Trabecular microfracture precedes cortical shell failure in the rat caudal vertebra under cyclic overloading.* Calcif Tissue Int, 2009. 85(2): p. 127-33.

# CHAPTER 4

# CONCLUSIONS AND FUTURE WORK

## Conclusions

The overall goal of this thesis was to investigate the properties of bone as it pertains to microdamage in aging and with anti-remodeling agents for treatment of osteoporosis. This was accomplished through two different aims. The first aim sought to determine the effects of aging on the bone matrix through microdamage progression. The mechanical function of bone depends a great deal on the properties of its local tissue matrix. While microdamage is known to accumulate naturally within the bone matrix, it is the ability of bone to resist microcrack growth and repair damage through remodeling that imparts the quality of long fatigue life *in vivo*. As such, an increase in the incidence of microdamage progression would reflect a compromised tissue matrix that has a reduced ability to resist microdamage progression. Decreased mechanical integrity of bone is present with the condition of osteoporosis as well. Current treatments (e.g. alendronate, ALN and raloxifene, RAL) seek to increase the bone mineral density (BMD) of bone in order to compensate for gross reductions in bone mass. However the mechanisms by which these therapies increase BMD, mainly inhibition of remodeling, are believed to alter the nature of bone at the local tissue level. Therefore, the second aim sought to determine the apparent properties of bone through biomechanical testing and the local tissue properties through derived material property calculations and microdamage quantification.

Aging was found to indicate increases in the average mineralization of trabecular bone as measured using micro-CT imaging. This reflects the age and the more homogeneous nature of the tissue itself since aging results in a more mature mineralized matrix as a consequence of imbalanced remodeling. More microdamage progression was found in old bone versus young bone presumably as a result of a decrease in the heterogeneity of the tissue matrix. Thus, the use of microdamage to assess the integrity of bone tissue matrix is shown to be both valid and reflective of age-related changes.

Combination treatment with RAL and ALN resulted in increased trabecular bone volume fraction which was associated with an increase in vertebral ultimate load. While no increases in derived material properties were found, improvements to the trabecular architecture by combination treatment were better than either RAL or ALN alone could affect. Consistent with studies from literature, no differences were found in overall preexisting and test-induced incidences of microdamage. However, OVX rats had more incidences of linear microdamage relative to diffuse and severe damage. Treatment with RAL and ALN together resulted in no such relative increase in linear damage. Since linear damage is associated more with risk of fracture than diffuse damage, this result suggests an improvement in the local tissue matrix properties.

Biomechanical testing of bones gives insight into the apparent level mechanical properties and by accounting for sample geometries and bone volume, can provide an estimation of material properties. This is a standard method for evaluating the effects of aging and drug therapies on extrinsic properties of bone. By creating microdamage *in vitro* and assessing the quantity and morphologies present, valuable information regarding the tissue level properties can be deduced. This method is a more powerful tool

that can be easily utilized in conjunction with biomechanical testing to provide insight into the underlying factors contributing to skeletal fragility and increased fractures.

## Future Work

To increase the power of using microdamage as a quantitative assessment of bone tissue matrix, improvements to the current studies have been considered. Measuring the characteristics of microcracks, such as crack length, crack depth, and area of damage, would provide new data that would enhance the methods used here. This would require the use of better image processing software than was used for this study. Non-invasive means for detecting microdamage would significantly improve the quantitative evaluation of the presence of microdamage. Limited means of doing this have been studied with the use of micro-CT imaging [1-3], but so far the results have not been much of an improvement over using fluorescent staining and histology. The main reason for this is the lack of specificity to the damage site that has made fluorescent chelating agents so useful. A promising technique is to use gold nanoparticles to localize to sites of damage, but this technique requires further work and is limited by the detection resolution of the micro-CT machine [4].

The use of finite element models would also enhance the results provided by mechanical testing and microdamage analysis. Previous work has validated a method for correlating stresses and strains to microdamage initiation in bovine [5-6], dog [7], and human trabecular bone. Application of this technique to the rat vertebrae would provide for further characterization of local tissue properties in a small animal model suitable for investigating bone disorders. This may require an adaptation of the technique in order to account for the structural nature of vertebrae (i.e. cortical shell and trabecular core)

compared to trabecular bone core samples. Accounting for the interplay between the cortex and trabeculae would provide for a more accurate and specific means of estimating local mechanical behavior. However, in order to characterize microdamage progression, non-linear models would be necessary to account for changes in the surrounding material and the redistribution of local stresses and strains [8-11]. Brief investigations into this avenue of study were conducted but further progress was halted by computational restrictions.

Another potential area of research involving HIV-associated bone loss would benefit greatly from a combined mechanical testing, microdamage quantification, and finite element modeling assessment of bone mechanical properties. With the development of improved HIV/AIDS treatments in recent decades, the life expectancy of HIV-infected patients has improved dramatically. One study found that osteopenia occurred in 67.5% of HIV-infected patients versus 25% of healthy adults and osteoporosis was present in 21.2% of HIV-infected patients versus 5% in healthy adults (n = 100 healthy adults, n = 80 HIV-infected adults) [12]. In fact many studies have raised the concern of fragility fractures associated with HIV-positive adults [13]. These results present potential opportunities for investigating the effects of HIV infection on bone apparent and local tissue properties in an effort to predict fragility fractures.

## References


1. Lee, T.C., et al., *Detecting microdamage in bone.* J Anat, 2003. 203(2): p. 161-72.

2. Wang, X., et al., *Detection of trabecular bone microdamage by micro-computed tomography.* J Biomech, 2007. 40(15): p. 3397-403.

3. Landrigan, M.D., et al., *Contrast-enhanced micro-computed tomography of fatigue microdamage accumulation in human cortical bone.* Bone, 2010.

4. Zhang, Z., R.D. Ross, and R.K. Roeder, *Preparation of functionalized gold nanoparticles as a targeted X-ray contrast agent for damaged bone tissue.* Nanoscale, 2010. 2(4): p. 582-6.

5. Nagaraja, S., T.L. Couse, and R.E. Guldberg, *Trabecular bone microdamage and microstructural stresses under uniaxial compression.* J Biomech, 2005. 38(4): p. 707-16.

6. Nagaraja, S., A.S. Lin, and R.E. Guldberg, *Age-related changes in trabecular bone microdamage initiation.* Bone, 2007. 40(4): p. 973-80.

7. O'Neal, J.M., et al., *One year of alendronate treatment lowers microstructural stresses associated with trabecular microdamage initiation.* Bone, 2010. 47(2): p. 241-7.

8. Kosmopoulos, V., C. Schizas, and T.S. Keller, *Modeling the onset and propagation of trabecular bone microdamage during low-cycle fatigue.* J Biomech, 2008. 41(3): p. 515-22.

9. Yang, Q.D., et al., *Fracture length scales in human cortical bone: the necessity of nonlinear fracture models.* Biomaterials, 2006. 27(9): p. 2095-113.

10. Stolken, J.S. and J.H. Kinney, *On the importance of geometric nonlinearity in finite-element simulations of trabecular bone failure.* Bone, 2003. 33(4): p. 494-504.

11. Kosmopoulos, V. and T.S. Keller, *Predicting trabecular bone microdamage initiation and accumulation using a non-linear perfect damage model.* Med Eng Phys, 2008. 30(6): p. 725-32.

12. Knobel, H., et al., *Osteopenia in HIV-infected patients: is it the disease or is it the treatment?* AIDS, 2001. 15(6): p. 807-8.

13. Amorosa, V. and P. Tebas, *Bone disease and HIV infection.* Clin Infect Dis, 2006. 42(1): p. 108-14.